

The Planck Scale from Top Condensation

Yang Bai^a, Marcela Carena^{a,b} and Eduardo Pontón^c

^a*Fermi National Accelerator Laboratory, P.O. Box 500, Batavia, IL 60510, USA*

^b*Enrico Fermi Institute, Univ. of Chicago, 5640 Ellis Ave., Chicago, IL 60637, USA*

^c*Department of Physics, Columbia University,
538 W. 120th St, New York, NY 10027, USA*

Abstract

We propose a scenario in which the Planck scale is dynamically linked to the electroweak scale induced by top condensation. The standard model field content, without the Higgs, is promoted to a 5D warped background. The only additional ingredient is a 5D fermion with the quantum numbers of the right-handed top. Localization of the zero-modes leads, at low energies, to a Nambu-Jona-Lasinio model that also stabilizes the radion field dynamically thus explaining the hierarchy between the Planck scale and $v_{EW} = 174$ GeV. The top mass arises dynamically from the electroweak breaking condensate. The other standard model fermion masses arise naturally from higher-dimension operators, and the fermion mass hierarchies and flavor structure can be explained from the localization of the zero-modes in the extra dimension. The model is easily consistent with the electroweak precision data, since the Kaluza-Klein scale is *predicted* to be about two orders of magnitude above the electroweak scale. This little hierarchy is a dynamical consequence of the radion stabilization mechanism and is free of fine-tuning. The model predicts a heavy (composite) Higgs with a mass of about 500 GeV and standard-model-like properties, and a vector-like quark with non-negligible mixing with the top quark and mass in the 1.6–2.9 TeV range. Both can be within the reach of the LHC. It also predicts a radion with a mass of a few GeV that is very weakly coupled to standard model matter.

1 Introduction

In the past couple of decades there has been a tremendous effort, both theoretical and experimental, to try to understand the electroweak scale. An important driving force has come from the desire to understand how this scale is related, if at all, to other scales in nature such as the Planck scale. Dynamical symmetry breaking through strong interactions provides a beautiful conceptual framework for understanding naturally hierarchically different scales. The analogy with the QCD interactions played a prominent role in the application of the idea to the generation of the electroweak (EW) scale itself, when the Technicolor model was introduced in the late 1970's [1, 2]. Fermion masses were later introduced via extended technicolor (ETC) [3, 4] (for recent developments see [5]). Because of the difficulty in generating a large top quark mass in the ETC theory, a more natural proposal where top quark condensation breaks the electroweak symmetry was first proposed in [6, 7, 8], and later developed in [9, 10, 11]. Fitting the observed top quark mass was finally possible in the context of the top seesaw model [12] (see [13] for a comprehensive study). More recently, extra-dimensional scenarios [14, 15, 16, 17] have led to a simple realization of the basic ingredients of Topcolor models [18]. For a review of strong dynamical electroweak symmetry breaking and an extended list of references, see [19].

In this paper we assume that the standard model (SM) fields propagate in a 5D *warped* background [20], resulting in strong interactions that lead to a simple picture where the EW symmetry is broken by a fermion-anti fermion condensate. The source of the strong interactions responsible for the condensate is related to the 5D $SU(3)_C$ QCD interactions, specifically to the gluon KK modes, which can easily be sufficiently strong to trigger the condensation. Our main observation is that the resulting vacuum energy in the presence of the condensate depends on the separation between the “ultraviolet” (UV) and “infrared” (IR) branes, L . This is because the KK gluon masses and the couplings of the condensing fermions to the KK gluons are L -dependent so that the vacuum energy in the presence of condensation is also L -dependent. Thus, a potential for the radion field is induced. Crucially, the vacuum energy has a minimum that naturally leads to an inter-brane distance parametrically larger than the 5D curvature scale. As a result, the Planck, the Kaluza-Klein (KK) and the electroweak scales are all related dynamically. It is widely appreciated that a complete solution to the hierarchy problem within warped scenarios [21] requires a specification of a radion stabilization mechanism. Notice that, unlike the well-known Goldberger-Wise mechanism for radion stabilization [22], we do not add by hand dynamics for the sole purpose of stabilizing the radion field. In this sense, our mecha-

nism is closer in spirit to the proposal of radion stabilization through Casimir energies [23]. We go beyond the previous proposals in that the stabilization of the distance between the branes is directly related to electroweak symmetry breaking (EWSB), and leads to a rather non-trivial link between various scales in the theory.

We illustrate the radion stabilization mechanism in a simple toy model in Section 2. The mechanism can be studied in detail within an effective Nambu-Jona-Lasinio (NJL) model [24] in the large N limit. We show, in particular, that the potential always has a well-defined minimum. The Planck/EW scale hierarchy is obtained provided a certain coupling is about 10% above a critical value. The size L is adjusted dynamically and one finds that, when the Planck/EW scale ratio is reproduced, the KK scale is predicted to be a factor of about 200 above the EW scale. Thus, the radion stabilization mechanism we propose not only explains the large hierarchy between the Planck and EW scales, but also the little hierarchy between the KK and EW scales. Furthermore, the relaxation of the radion field to the minimum of the potential energy ensures that typically only one of the fermions condenses, the one closest to the IR brane. In the context of the SM, the top quark is the most natural candidate to condense.

The realistic model described in Section 3 is extremely simple: the $SU(3)_C \times SU(2)_L \times U(1)_Y$ gauge fields and the SM fermion field content are supplemented by an additional quark field with the quantum numbers of the right-handed (RH) top quark, and are assumed to propagate in the bulk of a warped 5D space. There is no *fundamental* scalar field. We choose boundary conditions such that at energies below the KK scale, there is one *vector-like* fermion χ , in addition to the SM fermions. We assume that the SM fermion closest to the IR brane is one of the $SU(2)_L$ quark doublets (which is then identified as the left-handed (LH) third generation quark doublet). Its condensation partner is a linear combination of the RH top quark and χ_R , which is the most general and natural case allowed by the underlying 5D structure. Therefore, the EW symmetry is effectively broken by top condensation [11], and the fact that the top mass is of order the EW scale (and much larger than the other fermion masses) is a natural consequence. The fact that the condensate involves a linear combination of RH fields leads to a version of the top seesaw [12] that easily accommodates the observed top mass. In this sense, the model we propose can be regarded as a UV completion for the top condensation scenario, that also leads to a novel realization of the top seesaw scheme.

In Section 3, we also show how the EW scale and the top mass are obtained in the above model. We also present in some detail how the light fermion masses can arise from higher-

dimension operators involving the top and χ fields. Radion stabilization predicts that the KK scale is at about 35 TeV. The low-energy spectrum includes, besides the SM fermions and gauge bosons, a (composite) Higgs with a mass of 500 GeV and a vector-like quark that mixes with the top quark. In Section 4, we show that the EW constraints imply that the vector-like quark mass should be in the 1.6–2.9 TeV range. We also show that the radion field has a mass of a few GeV and a “decay constant” of order a few hundred TeV, which makes its detection challenging. The collider phenomenology of the present scenario is also briefly discussed. Section 5 contains our conclusions.

Finally, we provide two appendices with technical discussions. In Appendix A, we clarify how the strong coupling relevant to the physics of condensation is related to the strong coupling physics intrinsic to the 5D theory. We also estimate carefully the size of 4-fermion interactions that are expected to be present in the 5D theory, and that give rise, in the present scenario, to the masses of the SM fermions other than the top. We collect in Appendix B several formulas that are relevant for the EW precision analysis.

2 Condensates and Radion Stabilization

We start by considering the simplest toy model that displays the main features of the radion stabilization mechanism. This will allow us to understand the main idea in a simple setting. A fully realistic implementation is considered in Section 3.

2.1 $SU(N_c)$ with Two Flavors

Consider an $SU(N_c)$ gauge theory (to be identified later with the color group) in the AdS₅ background

$$ds^2 = e^{-2ky} \eta_{\mu\nu} dx^\mu dx^\nu - dy^2, \quad (1)$$

where μ runs over the 4D noncompact directions and $0 \leq y \leq L$. We also consider two bulk fermions, Ψ_1 and Ψ_2 , in the fundamental representation of $SU(N_c)$. Their boundary conditions are chosen so that one gives rise to a LH zero-mode, ψ_{1L} , while the other gives rise to a RH zero-mode, ψ_{2R} . Here we are mainly interested in the physics of these fermion zero-modes which have profiles given by

$$f_c(y) = \sqrt{\rho_c} e^{(\frac{1}{2}-c)ky}, \quad (2)$$

where

$$\rho_c \equiv \frac{(1-2c)kL}{e^{(1-2c)kL} - 1} \quad (3)$$

is the normalization factor, and c stands for c_1 or c_2 , which parametrize the fermion 5D mass terms in units of the curvature scale k . Our conventions are such that, independently of chirality, the zero-modes are localized near the UV (IR) brane for $c > 1/2$ ($c < 1/2$). Tree-level exchange of the *first-level* gauge KK mode leads to 4-fermion operators of the form

$$-\frac{g_{c_1}g_{c_2}}{M_{\text{KK}}^2}(\bar{\psi}_{1L}T^A\gamma^\mu\psi_{1L})(\bar{\psi}_{2R}T^A\gamma^\mu\psi_{2R}) = \frac{g_{c_1}g_{c_2}}{M_{\text{KK}}^2}(\bar{\psi}_{1L}\psi_{2R})(\bar{\psi}_{2R}\psi_{1L}) + \mathcal{O}(1/N_c) , \quad (4)$$

where T^A are the $SU(N_c)$ generators, the parenthesis indicates how the color contractions are performed, and the right-hand side is obtained by Fierz rearrangement. Also, M_{KK} is the lightest KK gluon mass and g_c is its coupling to a fermion with localization parameter c , given by the overlap integral

$$g_c = \frac{g_5}{L^{3/2}} \int_0^L dy |f_c(y)|^2 f_G^{(1)}(y) , \quad (5)$$

where g_5 is the 5D gauge coupling, and $f_G^{(1)}(y)$ is the first-level KK gluon wavefunction.¹ Other operators that involve only LH or only RH fermions will play no role in the following discussion (notice they have the “wrong” sign to spontaneously break the Lorentz symmetry, as discussed in [25]). Also, in the 5D effective theory there are local 4-fermion interactions (suppressed by the cutoff of the 5D theory, Λ). We argue in detail in Appendix A that the effects due to these four-fermion interactions are expected to be subdominant compared to those obtained by integrating out the gauge KK modes.

The 4-fermion interaction due to gauge boson exchange, Eq. (4), is always attractive (i.e. $g_{c_1}g_{c_2} > 0$) and, if sufficiently strong, can lead to a fermion-antifermion condensate [7, 8] and a low-energy scalar degree of freedom [11], as reviewed below. It is important to notice that one can also consider the 4-fermion interactions induced by integrating the second and higher gauge KK modes out. However, it is easy to check that the relevant couplings, analogous to Eq. (5), are significantly smaller than the one associated with the first-level gauge KK mode. This can be understood from the oscillating behavior of the heavier gauge KK mode wavefunctions, which generally leads to cancellations. One can also consider the 4-fermion interactions among the *fermion* KK modes that arise when heavier KK gauge bosons are integrated out. But

¹We define all wavefunctions so that the normalization reads $(1/L) \int_0^L dy |f(y)|^2 = 1$, without warp factors.

again, the associated couplings are significantly smaller than Eq. (5). As will be explained in Subsection 2.4, the largest coupling is only slightly above the critical value for the condensation to happen. As a result we do not expect fermion condensation in any of the above “KK channels”. This should be contrasted to the situation in flat space, where all non-vanishing couplings among KK modes are equal, and condensation happens in all channels that exist below the cutoff of the 5D theory [15].² We therefore concentrate on the 4-fermion operators that involve the lightest fermions and arise from exchange of the lightest gauge KK mode. This can be studied in the 4D effective theory valid below the KK scale. Since our main interest is in how this well-known condensation mechanism can also stabilize the radion and how the compactification and condensation scales are related, we start by establishing the dependence of the relevant parameters on L .

2.2 L -dependence of Microscopic Parameters

Both the coupling g_c and the KK scale M_{KK} depend on the size of the extra dimension L . In order to find an analytical expression for this dependence, we resort to the following trick: it is easy to obtain an analytical expression for the coefficient of the 4-fermion operator, Eq. (4), induced by integrating out the full tower of gluon KK modes, using propagator techniques [26]. On the other hand, these effects are saturated to a very good approximation by the lightest KK gluon, which is the one that concerns us. This observation allows us to obtain an approximate expression for g_c in Eq. (5). The effects of the complete KK tower sum up to

$$\sum_{n=1}^{\infty} \frac{g_n^2}{M_n^2} = \frac{g_5^2 k}{k^2 e^{-2kL}} \left[f_1(c_1, c_2) - \frac{f_2(c_1, c_2)}{kL} + \frac{1}{4k^2 L^2} \right], \quad (6)$$

where g_n is the coupling to the fermion zero-modes of the n -th KK gluon with mass M_n . When $c_{1,2} < 1/2$ (i.e. fermions localized near the IR brane), one has

$$f_1(c_1, c_2) = \frac{(1 - 2c_1)(1 - 2c_2)(3 - c_1 - c_2)}{2(3 - 2c_1)(3 - 2c_2)(2 - c_1 - c_2)}, \quad (7)$$

$$f_2(c_1, c_2) = \frac{45 - 28[c_1(3 - c_1) + c_2(3 - c_2)] + 16c_1c_2(3 - c_1)(3 - c_2)}{2(3 - 2c_1)^2(3 - 2c_2)^2}, \quad (8)$$

where exponentially small effects have been neglected.

²Ref. [16] considered a warped space analog. However, no fermion bulk masses were considered and, since for $c = 0$ the fermion KK wavefunctions reduce to sines and cosines, a situation similar to flat space ensues. For arbitrary c -parameters, however, the condensation occurs only among the lightest fermions (zero-modes, or ultra-light modes, as described in Section 3), due to exchange of the first-level gauge KK modes.

The lightest KK gluon mass is given by

$$M_{\text{KK}} = x_1 k e^{-kL} , \quad (9)$$

where $x_1 \approx 2.45$ has a very mild dependence on L that, for simplicity, we will ignore in the following. Using the fact that Eq. (6) is almost saturated by this lightest mode, and comparing to Eq. (4), we find

$$g_{c_1} g_{c_2} \approx g_5^2 k x_1^2 \left[f_1(c_1, c_2) - \frac{f_2(c_1, c_2)}{kL} + \frac{1}{4k^2 L^2} \right] . \quad (10)$$

Indeed, it is easy to check numerically that $g_{c_1} g_{c_2}$ computed from Eqs. (5) or (10) agree to better than the per mille level for the parameters of interest.

We also point out that the functions $f_1(c_1, c_2)$ and $f_2(c_1, c_2)$ are positive definite, a fact that will be used below. This can be checked explicitly when $c_{1,2} < 1/2$ and Eqs. (7) and (8) apply. When $c_i > 1/2$, these two functions become exponentially small.

2.3 Radion Potential

The 4-dimensional effective theory can lead to a potential for the radion through the L -dependence of M_{KK} and $g_{c_1} g_{c_2}$, as given in the previous subsection. As we will see, such a potential is intimately connected to the formation of a condensate $\langle \bar{\psi}_{1L} \psi_{2R} \rangle$ in a NJL model with the 4-fermion interactions given in Eq. (4). If the coupling in Eq. (10) is sufficiently large, a nontrivial condensate forms and gives rise to a scalar fermion-antifermion bound state. The simplest way to study this phenomenon is by rewriting the 4D theory including the 4-fermion interactions of Eq. (4), in terms of an auxiliary ‘‘Higgs’’ field, H , as [11]

$$\mathcal{L}_4 = i\bar{\psi}_{1L} \not{D} \psi_{1L} + i\bar{\psi}_{2R} \not{D} \psi_{2R} - M_{\text{KK}}^2 H^\dagger H + (g_\psi H \bar{\psi}_{1L} \psi_{2R} + \text{h.c.}) , \quad (11)$$

where D is the gauge covariant derivative with respect to the zero-mode gluon, and we have omitted the gluon kinetic term for simplicity. By integrating out the auxiliary field H the original Lagrangian is recovered, with the identification $g_\psi^2 = g_{c_1} g_{c_2} > 0$. We should regard the Lagrangian (11) as holding at the scale M_{KK} . Renormalization group running to lower scales leads to

$$\begin{aligned} \mathcal{L}_4(\mu) = & \mathcal{Z}_L i\bar{\psi}_{1L} \not{D} \psi_{1L} + \mathcal{Z}_R i\bar{\psi}_{2R} \not{D} \psi_{2R} + (\mathcal{Z}_{g_\psi} g_\psi H \bar{\psi}_{1L} \psi_{2R} + \text{h.c.}) \\ & + \mathcal{Z}_H \partial_\mu H^\dagger \partial^\mu H - m_H^2 H^\dagger H - \frac{\lambda}{2} (H^\dagger H)^2 , \end{aligned} \quad (12)$$

which shows that a scalar kinetic term is induced, and H can be thought as a dynamical degree of freedom below the scale M_{KK} . Furthermore, the Higgs squared mass parameter, that starts out positive at the M_{KK} scale, can be driven to negative values through radiative effects. If we ignore the effects of the Higgs self-interactions, the running arises from fermion loops and leads to

$$m_H^2 \approx M_{\text{KK}}^2 \left[1 - \frac{g_\psi^2 N_c}{8\pi^2} \left(1 - \frac{\mu^2}{M_{\text{KK}}^2} \right) \right], \quad \lambda \approx \frac{g_\psi^4 N_c}{8\pi^2} \ln \left(\frac{M_{\text{KK}}^2}{\mu^2} \right), \quad (13)$$

which indicates that H acquires a non-vanishing vacuum expectation value (VEV) provided

$$g_\psi^2 > G_c^2 \equiv \frac{8\pi^2}{N_c}. \quad (14)$$

As discussed above, the parameters that determine this VEV depend on the size of the extra dimension so that we effectively obtain a scalar potential for $\langle H \rangle$ and L , that should be minimized simultaneously. We rewrite this potential as

$$\begin{aligned} V(H, L) &= \bar{m}_H^2(L) H^\dagger H + \frac{\bar{\lambda}(L)}{2} (H^\dagger H)^2 \\ &= \frac{\bar{\lambda}(L)}{2} \left[H^\dagger H + \frac{\bar{m}_H^2(L)}{\bar{\lambda}(L)} \right]^2 - \frac{\bar{m}_H^4(L)}{2\bar{\lambda}(L)}, \end{aligned} \quad (15)$$

where, as a result of 5D general covariance, the radion dependence enters only through the (renormalized) parameters ³

$$\bar{m}_H^2 = \frac{m_H^2}{\mathcal{Z}_H}, \quad \bar{\lambda} = \frac{\lambda}{\mathcal{Z}_H^2}, \quad (16)$$

where

$$\mathcal{Z}_H = \frac{N_c g_\psi^2}{16\pi^2} \ln \left(\frac{M_{\text{KK}}^2}{\mu^2} \right). \quad (17)$$

We see that a radion potential is induced only when the condition (14) is fulfilled so that $\langle H^\dagger H \rangle = -\bar{m}_H^2/\bar{\lambda}$. Referring to Eq. (10) and given that the function $f_1(c_1, c_2)$ is positive definite, as mentioned above, we conclude that the condensate will form provided

$$g_5^2 k x_1^2 f_1(c_1, c_2) > G_c^2, \quad (18)$$

³Parameters associated with the gauge and fermion sectors also depend on L , but do not contribute to the radion potential as long as these fields do not acquire VEV's, which we assume to be the case.

which will occur whenever the fermions are sufficiently localized towards the IR brane. The reason is simply that the last two terms in Eq. (10) vanish as $kL \rightarrow \infty$, and therefore there is always a region where $g_{c_1}g_{c_2} > G_c^2$.⁴ Assuming that the inequality (18) is satisfied, and noting that $f_2(c_1, c_2)$ is also positive definite, we see that there is a critical value, L_c , defined by

$$g_5^2 k x_1^2 \left[f_1(c_1, c_2) - \frac{f_2(c_1, c_2)}{kL_c} + \frac{1}{4k^2 L_c^2} \right] = G_c^2, \quad (19)$$

such that for $L > L_c$ the condensate forms. It is then clear from the form of $V(H, L)$ that when $L > L_c$ and imposing $\partial V/\partial H = 0$ [i.e. $\langle H^\dagger H \rangle = -\bar{m}_H^2/\bar{\lambda}$], $\partial V/\partial L$ receives contributions only from the second term in Eq. (15). Thus, the radion potential is simply given by

$$\begin{aligned} V_{\text{eff}}(L) &= -\frac{\bar{m}_H^4}{2\lambda} \theta(L - L_c) \\ &\approx -\frac{M_{\text{KK}}^4 \left(\frac{1}{G_c^2} - \frac{1}{g_\psi^2} \right)^2}{\frac{N_c}{4\pi^2} \log \frac{M_{\text{KK}}^2}{\mu^2}} \theta(L - L_c), \end{aligned} \quad (20)$$

where $\theta(x)$ is the Heaviside step function, equal to 1 for $x \geq 0$ and zero otherwise. The renormalization scale μ should be taken of the order of the Higgs condensate: $\mu \sim v_{\text{EW}} < M_{\text{KK}}$. In Eq. (20) we neglected the term μ^2/M_{KK}^2 in m_H^2 [see Eq. (13)] since it is a negligible effect. We observe that $V_{\text{eff}}(L)$ is *negative* and vanishes both for $L < L_c$ and for $L \rightarrow \infty$ (for small L there is no condensate, hence no radion potential, while for large L , M_{KK} goes to zero exponentially). Therefore, the potential always has a minimum for some $L > L_c$ and stabilizes the radion whenever the condition (18) is satisfied. The radion potential is shown in Fig. 1.

It should be noticed that the existence of this minimum is rather robust: the vanishing of the potential at small L is due to the 4-fermion interaction turning subcritical, while the vanishing at $L \rightarrow \infty$ is a consequence of the fact that in the uncompactified limit, 5D general covariance forbids non-derivative terms that involve the radion field. The latter property is also important in forbidding *arbitrary* additional terms in the radion potential. In our case, the crucial point is that the radion is related to the higher-dimensional gravity multiplet. Notice also that the potential at the minimum is of order the EW scale, and we expect the gravitational backreaction on the warped background to be small. However, we must assume that there is an additional contribution to the vacuum energy that makes the 4D cosmological constant slightly positive (the usual cosmological constant fine-tuning problem), as indicated by observation. As

⁴Since $f_2(c_1, c_2) > 0$, the opposite inequality, $g_5^2 k x_1^2 f_1(c_1, c_2) < G_c^2$ can lead to a condensate only for $kL \ll 1$, when the third term in Eq. (10) can dominate. We do not consider such a possibility here.

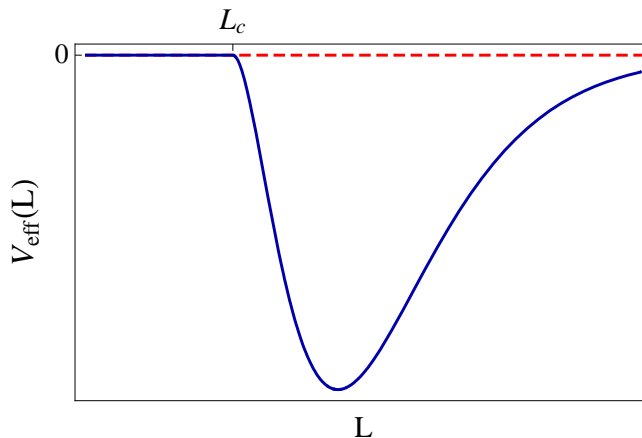


Figure 1: Radion potential, Eq. (20).

discussed in [23], a “mismatch” between the 5D cosmological constant and brane tensions that, when added to the contribution from the condensation, can make the net 4D vacuum energy nearly vanishing, leads to an additional radion-dependent contribution. Such a potential still vanishes at large L . It is possible to have a long-lived metastable minimum at a position close to the minimum of Eq. (20), that arises from the potential in Eq. (20) plus a contribution that behaves like an inverse power-law in the radion field, as would be expected from the above-mentioned mismatch.

2.4 Scales: Leading Order Analysis

We now explore the connection between the dynamically determined size of the extra dimension and the Higgs condensate:

$$\langle H \rangle \equiv v_{\text{EW}} = \sqrt{-\frac{\bar{m}_H^2}{\lambda}} = \frac{M_{\text{KK}}}{\sqrt{2}} \sqrt{\frac{1}{G_c^2} - \frac{1}{g_\psi^2}}. \quad (21)$$

Here we neglected, as before, the effects of the Higgs self-interactions. It is useful to define the functions

$$\bar{f}_i = g_5^2 k x_1^2 f_i(c_1, c_2), \quad \text{for } i = 1, 2, \quad (22)$$

where the $f_i(c_1, c_2)$ were defined in Eqs. (7) and (8). In terms of these, the condition that ensures that a condensate exists, Eq. (18), is simply $\bar{f}_1 > G_c^2$. Since, as we will see, the radion is stabilized at values $kL \gg 1$, we will neglect the third term in Eq. (10) in order to simplify the following analytical expression. We will include the full expression in the numerical studies.

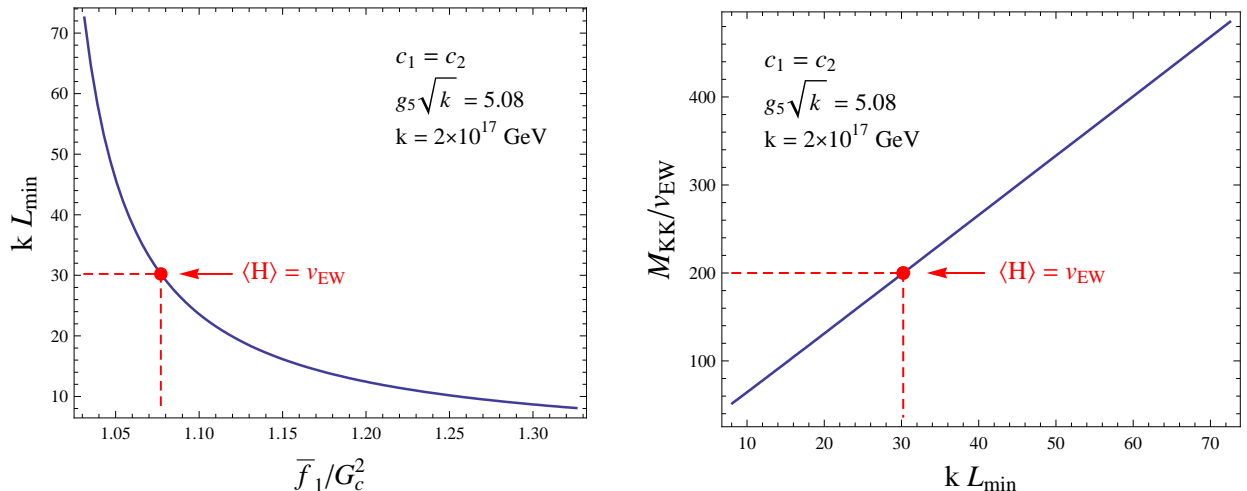


Figure 2: Left panel: kL_{\min} as a function of \bar{f}_1/G_c^2 [see Eqs. (22) and (23)]. The variation in \bar{f}_1 is obtained by varying $c_1 = c_2$ for fixed “underlying” KK gluon coupling $g_5\sqrt{k} = 5.08$. Right panel: Ratio of the KK scale to the Higgs VEV as a function of kL_{\min} . The red dots indicate the point where the Higgs VEV is at the electroweak scale, v_{EW} . The choice of $g_5^2 k$ is such that at this point we reproduce the “observed” $\alpha_s(\mu = M_{KK}) \approx 0.068$, where $M_{KK} \approx 35$ TeV.

The minimum of the radion potential, Eq. (15), is then given by

$$\begin{aligned}
kL_{\min} &= \frac{\bar{f}_2}{\bar{f}_1 - G_c^2} + \frac{\sqrt{1 + \frac{2\bar{f}_1}{G_c^2\bar{f}_2}(\bar{f}_1 - G_c^2)} - 1}{\frac{2\bar{f}_1}{G_c^2\bar{f}_2}(\bar{f}_1 - G_c^2)} \\
&\approx \frac{\bar{f}_2}{\bar{f}_1 - G_c^2} + \frac{1}{2}, \tag{23}
\end{aligned}$$

where the second equality holds when $\bar{f}_1/G_c^2 - 1 \ll 1$. In this case we get $kL_{\min} \gg 1$. To get a more quantitative idea, we note that \bar{f}_2/\bar{f}_1 lies between 2 and 3 for $-1 < c_1 = c_2 < 0$. Thus, if \bar{f}_1 is within 10% of G_c^2 one gets kL_{\min} of order 20 – 30, roughly what is required to explain the Planck-weak scale hierarchy.

Note also that once kL_{\min} is determined by the above dynamical mechanism, the low-energy gauge coupling is computed from

$$\alpha_s = \frac{g_5^2}{4\pi L_{\min}}. \tag{24}$$

If we are aiming at explaining the Planck-weak scale hierarchy, so that $kL_{\min} \sim 33 - 34$, and identify α_s with the strong coupling constant, we see that the “fundamental” KK gluon coupling

is determined to be $\sqrt{g_5^2 k} \sim 6$, although its precise value depends on the actual matching scale M_{KK} , both through the value of kL_{min} and the RG running of α_s up to the KK scale.

In the left panel of Fig. 2 we show kL_{min} as a function of \bar{f}_1/G_c^2 . We obtain different values of \bar{f}_1 by varying the localization of the fermions. For illustration purposes, we took $c_1 = c_2$, but the situation is similar in the more general case. We fix $g_5^2 k$ so that α_s has the correct⁵ value at M_{KK} when the condensate has the correct value, $\langle H \rangle = v_{\text{EW}} = 174$ GeV. These two requirements uniquely fix $g_5^2 k$ and \bar{f}_1 (for $c_1 = c_2$ and $k = 2 \times 10^{17}$ GeV we find $c_1 = -0.62$). The size of the extra-dimension, kL , is then fixed by the minimization of the potential to be $kL_{\text{min}} \approx 30$. The hierarchy between the weak and Planck scales is explained when \bar{f}_1 is within 10% of G_c^2 , a relatively moderate tuning.⁶ The KK scale is then predicted to be 35 TeV (see right panel of Fig. 2). Interestingly, the radion is stabilized at a point where the actual coupling of the KK gluon to fermions, $g_\psi^2 = g_{c_1} g_{c_2}$ [see Eq. (10)], is rather close to the critical coupling G_c^2 . Specifically, we get

$$g_\psi^2 \approx G_c^2 + \frac{(\bar{f}_1 - G_c^2)^2}{2\bar{f}_2}, \quad (25)$$

which gives $g_\psi^2/G_c^2 - 1 \approx 10^{-3}$. Notice that g_ψ^2 is closer to G_c^2 than the original 10% input by a factor $(g_\psi^2 - G_c^2)/(\bar{f}_1 - G_c^2) \approx (\bar{f}_1 - G_c^2)/(2\bar{f}_2) = \mathcal{O}(1/\bar{f}_2)$, which is small because $\bar{f}_2 \sim g_5^2 k x_1^2 \gg 1$, a consequence of the underlying strong dynamics. This accounts for the factor of about 1/100 of additional suppression in the difference $g_\psi^2 - G_c^2$. As a result, a relatively large hierarchy between v_{EW} and M_{KK} is predicted:

$$v_{\text{EW}} \approx M_{\text{KK}} \left(\frac{\bar{f}_1 - G_c^2}{2G_c^2} \right) \sqrt{\frac{1}{\bar{f}_2}}, \quad (26)$$

as shown on the right panel of Fig. 2. In that figure we also marked the point where $\langle H \rangle = v_{\text{EW}}$, which is associated with a KK scale $M_{\text{KK}} \approx 35$ TeV (and $kL_{\text{min}} \approx 30.27$). We stress that the hierarchy between M_{KK} and v_{EW} of about 200 requires only a moderate 10% tuning, so that there is essentially no little hierarchy problem. This is a consequence of the radion stabilization mechanism that relaxes L to a point where g_ψ^2 is driven very close to the critical value. This

⁵We use the RG equation with the SM field content plus one additional $SU(2)_L$ singlet quark with a mass of a ~ 2 TeV, for reasons discussed in Section 3, to obtain the value of $\alpha_s(M_{\text{KK}})$ from $\alpha_s(M_Z)$.

⁶Defining the sensitivity by $\mathcal{S} = \partial \log v_{\text{EW}} / \partial \log \bar{f}_1$ [27], we obtain $\mathcal{S} \approx (\bar{f}_2/\bar{f}_1)(\bar{f}_1/G_c^2 - 1)^{-2}$. As argued in [28], the fine-tuning should be obtained by comparison with the typical sensitivity, defined as an appropriate average, which in our case is $\bar{\mathcal{S}} = 12\bar{f}_2 G_c^4 / [(\bar{f}_{\text{max}} - G_c^2)^2 (3\bar{f}_{\text{max}} + G_c^2)]$. For $|c_1|, |c_2| \leq 1$, $\bar{f}_{\text{max}} \approx 1.35 G_c^2$, and we find $\mathcal{S}/\bar{\mathcal{S}} \approx 10$, which corresponds to a 10% fine-tuning.

also implies that generically only the fermions closest to the IR brane, which have the strongest couplings to the first-level KK gluon, will condense. Other fermions which are somewhat further away from the IR brane will have subcritical couplings. This is also true for the fermion KK modes, which have couplings to the KK gluons that are smaller from those of the lightest fermion modes (see comments in the last paragraph of Subsection 2.1).

2.5 Scales: Improved Analysis

To estimate more precisely the renormalized fermion Yukawa coupling \bar{g}_ψ and the Higgs quartic coupling $\bar{\lambda}$, hence the Higgs boson mass, at a low energy scale μ , we include the SM gauge couplings and Higgs self-interactions into the renormalization group (RG) equations for \bar{g}_ψ and $\bar{\lambda}$. At one loop order these are [11]

$$16\pi^2 \frac{d\bar{g}_\psi}{d\ln\mu} = \bar{g}_\psi \left[\frac{9}{2} \bar{g}_\psi^2 - 8 \bar{g}_3^2 - \frac{9}{4} \bar{g}_2^2 - \frac{17}{12} \bar{g}_Y^2 \right], \quad (27)$$

$$16\pi^2 \frac{d\bar{\lambda}}{d\ln\mu} = 12 \left[\bar{\lambda}^2 + (\bar{g}_\psi^2 - \frac{1}{4} \bar{g}_Y^2 - \frac{3}{4} \bar{g}_2^2) \bar{\lambda} + \frac{1}{16} \bar{g}_Y^4 + \frac{1}{8} \bar{g}_Y^2 \bar{g}_2^2 + \frac{3}{16} \bar{g}_2^4 - \bar{g}_\psi^4 \right], \quad (28)$$

while the SM gauge couplings satisfy

$$16\pi^2 \frac{d\bar{g}_i}{d\ln\mu} = b_i \bar{g}_i^3, \quad (29)$$

with

$$b_3 = -7 + \frac{2}{3} n_f, \quad b_2 = -\frac{19}{6} + \frac{1}{6} n_s, \quad b_1 = \frac{41}{6} + \frac{1}{6} n_s + \frac{8}{27} n_f. \quad (30)$$

Here we introduced n_s and n_f to take into account additional particles beyond the standard model, which will be discussed in a realistic model in Section 3. We will choose $n_s = 1$ for $\mu > 10$ TeV and $n_s = 0$ for $\mu \leq 10$ TeV, while $n_f = 1$ for $\mu > 2$ TeV and $n_f = 0$ for $\mu \leq 2$ TeV. This corresponds to having one additional Higgs doublet at 10 TeV and one additional top quark-like fermion at 2 TeV. To solve the RG equations, we use the ‘‘compositeness conditions’’ $\bar{g}_\psi = \infty$ and $\bar{\lambda} = \infty$ at the M_{KK} scale [11], which corresponds to having vanishing Higgs kinetic term and quartic coupling at the compositeness scale, $M_{\text{KK}} \approx 35$ TeV. In the following numerical studies the SM gauge couplings at M_Z are taken from the PDG [29], while their experimental errors are neglected since they are expected to be small compared to the theoretical uncertainties.

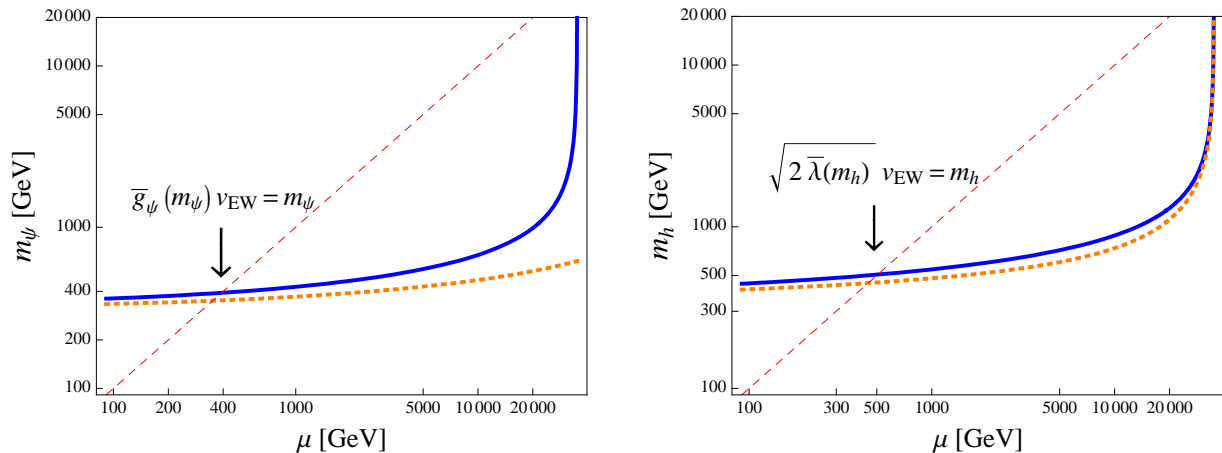


Figure 3: Left panel: the fermion mass m_ψ as a function of the running scale μ . Right panel: the Higgs boson mass m_h as a function of μ . The solid (blue) line is for the boundary condition $\bar{g}_\psi(M_{\text{KK}}) = \infty$, while the dotted (orange) line is for the boundary condition $\bar{g}_\psi(M_{\text{KK}}) = \sqrt{4\pi}$. The intersection with the dashed (red) line, $m(\mu) = \mu$, determines the particle masses: $m_\psi = 375 \pm 25$ GeV and $m_h = 475 \pm 25$ GeV.

In Fig. 3, we show the fermion and the Higgs boson masses as functions of the energy scale μ , that follow from integration of Eqs. (27) and (28). We use the mass-shell condition $m(\mu = m_{\text{phys}}) = m_{\text{phys}}$ to define the physical mass. To estimate the error in our perturbative calculation of a strongly coupled theory, we report two boundary conditions for \bar{g}_ψ . One is $\bar{g}_\psi(M_{\text{KK}}) = \infty$ as shown in the solid (blue) line, while the other is $\bar{g}_\psi(M_{\text{KK}}) = \sqrt{4\pi}$ as shown in the dotted (orange) line. In this way, we find a fermion mass of $m_\psi = 375 \pm 25$ GeV, while the Higgs boson mass is $m_h = 475 \pm 25$ GeV. The actual masses of the new fermion and the new Higgs doublet are not important for the numerical solutions of the RG equations. If we neglect the effects from the new particle's contributions by choosing $n_s = n_f = 0$ for all scales in Eq. (29), the final values for m_ψ and m_h are only changed by around 1 GeV, and hence contribute negligibly to the errors of m_ψ and m_h . However, the RG improved masses of the new fermion and Higgs doublet are relevant to study the phenomenological consequences of this scenario.

3 The Planck and EW Scales from a Top Seesaw

Having discussed the mechanism for condensation and radion stabilization in Section 2, we now turn our attention to a realistic implementation where the above condensation mechanism

is responsible for EW symmetry breaking and the generation of all SM fermion masses. The fermions that condense must then carry $SU(2)_L \times U(1)_Y$ quantum numbers. One possibility is to consider a fourth generation as done recently in Ref. [17]. This leads to a Higgs mass of order a TeV, and a fourth generation fermion with a mass in the several hundred GeV range. The light fermion masses can be generated from local 4-fermion operators suppressed by the cutoff scale Λ [see Eq. (52) below], as discussed in Subsection 3.3 below. However, such effects are naturally suppressed, and can hardly be expected to generate the top quark mass (see Subsection 3.3 and Appendix A). We therefore consider a scenario where the top quark takes an active role in the condensation mechanism. The EW scale is then closely connected to top condensation [11]. As we will see, our setup leads naturally to a Top Seesaw [12] structure, so that a top quark parametrically lighter than the Higgs can be easily accommodated.

3.1 The Model

In more detail, the SM model is embedded into 5D fields propagating on the background of Eq. (1) as follows. We concentrate on the “top sector”, which arises from an $SU(2)_L$ doublet 5D fermion, Ψ_{Q_L} , with hypercharge 1/3, plus *two* $SU(2)_L$ singlet 5D fermions, Ψ_1 and Ψ_2 , with hypercharge 4/3.⁷ This setup has exactly one additional $SU(2)_L$ singlet compared to the standard minimal construction.⁸ The boundary conditions are chosen so that Ψ_{Q_L} has a LH zero-mode, $Q_L = (t_L, b_L)$. Since Ψ_1 and Ψ_2 have the same quantum numbers, we can write a general two by two 5D Dirac mass matrix for them. Such a mass matrix can always be diagonalized, but the boundary conditions in the basis where the 5D mass matrix is diagonal need not be of the simple $(-, +)$ or $(+, +)$ type for the two individual fields. Rather, one should allow for general linear combinations of the fields with the same quantum numbers to be assigned Neumann or Dirichlet boundary conditions. From now on, we will define Ψ_1 and Ψ_2 as *Dirac mass eigenstates* with Dirac masses written as $c_1 k$ and $c_2 k$ respectively, while the Dirac mass associated with the doublet is written as $c_Q k$. The boundary conditions for the $SU(2)_L$ singlets are described in more detail below.

We choose one linear combination of Ψ_1 and Ψ_2 to have a RH zero-mode, while the orthogonal linear combination has an ultralight Dirac KK mode. The low-energy (i.e. below the

⁷In spite of the notation, these fields should not be identified with the fields of the toy model of Subsection 2.1.

⁸There is no corresponding enlargement of the field content in the first two generations. In summary, we simply take the 5D SM field content without the Higgs field and add a single 5D fermion with the quantum numbers of the RH top quark. A Chern-Simons term to cancel anomalies resulting from the compactification needs to be added [15], but it has no impact on the physics we are interested in.

KK scale) singlet fermions are denoted by t_R , χ_L and χ_R . In general, t_R lives in both RH 5D fermions, Ψ_{1R} and Ψ_{2R} , as does the ultralight Dirac KK mode, χ . The KK decomposition in the RH sector reads

$$\begin{aligned}\Psi_{1R}(x, y) &= \frac{e^{\frac{3}{2}ky}}{\sqrt{L}} [h_1(y) t_R(x) + k_1(y) \chi_R(x) + \dots] , \\ \Psi_{2R}(x, y) &= \frac{e^{\frac{3}{2}ky}}{\sqrt{L}} [h_2(y) t_R(x) + k_2(y) \chi_R(x) + \dots] ,\end{aligned}\quad (31)$$

where \dots represent higher KK modes, and $h_i(y)$, $k_i(y)$ are the wavefunction profiles for t_R and χ_R , respectively. The ‘‘misalignment’’ between the boundary conditions and the general Dirac mass matrix for Ψ_1 and Ψ_2 is parametrized by an angle θ . We require $\cos\theta \Psi_{1R} + \sin\theta \Psi_{2R}$ to obey $(+, +)$ boundary conditions, so that it contains the zero-mode t_R , while the orthogonal combination $-\sin\theta \Psi_{1R} + \cos\theta \Psi_{2R}$ is assigned $(-, +)$ boundary conditions and contains the ultralight mode χ_R .

For the zero-mode t_R , the wavefunction profiles are

$$h_1(y) = \frac{\cos\theta}{\sqrt{a(c_1, c_2)}} e^{(\frac{1}{2}-c_1)ky} , \quad h_2(y) = \frac{\sin\theta}{\sqrt{a(c_1, c_2)}} e^{(\frac{1}{2}-c_2)ky} . \quad (32)$$

Here $a(c_1, c_2)$ is a dimensionless parameter that normalizes the 4D fermion wavefunction according to $\frac{1}{L} \int_0^L dy (|h_1(y)|^2 + |h_2(y)|^2) = 1$, and is given by

$$a(c_1, c_2) = \frac{\cos^2\theta}{\rho_{c_1}} + \frac{\sin^2\theta}{\rho_{c_2}} , \quad (33)$$

where ρ_c was defined in Eq. (3) [ρ_{c_1} and ρ_{c_2} are precisely the normalization factors of the zero-modes of 5D Dirac fermions obeying $(+, +)$ boundary conditions]. For $c_1, c_2 < -1/2$, the solutions for the wavefunction profiles of the ultralight KK mode, χ_R , are approximately

$$k_1(y) \approx -\tan\theta \sqrt{\frac{\rho_{c_1}}{\rho_{c_2}}} h_1(y) , \quad k_2(y) \approx \cot\theta \sqrt{\frac{\rho_{c_2}}{\rho_{c_1}}} h_2(y) , \quad (34)$$

where the approximation is very good even for y 's far from the IR brane. Again the wavefunction of χ_R is properly normalized here. The ultralight Dirac mass, that marries the χ_L and χ_R fields, is

$$m_d \approx \sqrt{\frac{(1+2c_1)(1+2c_2) [(2c_2-1) e^{(1+2c_2)kL} + (2c_1-1) \tan^2\theta e^{(1+2c_1)kL}]}{1+2c_1 + (1+2c_2) \tan^2\theta}} k e^{-kL} . \quad (35)$$

This formula is valid for c_2 less than $-1/2$ and when c_1 and c_2 are not too close to each other. It shows the Dirac mass to be exponentially smaller than $\tilde{k} \equiv k e^{-kL}$. For $\theta = 0$, the ultralight mode arises purely from Ψ_{2R} , and has a mass $m_d \approx \sqrt{4c_2^2 - 1} e^{(\frac{1}{2}+c_2)kL} \tilde{k}$.

The couplings of the lightest KK gluon to the RH 4D fermions can be read from the 5D fermion covariant kinetic terms after replacing them by their KK decomposition, Eq. (31), as well as the gluon one. Noticing that $h_i(y)$ and $k_i(y)$ are proportional to the same exponential function, these couplings take the form

$$\begin{aligned} & \frac{g_{c_1}}{\rho_{c_1}\rho_{c_2} a(c_1, c_2)} (\bar{t}_R \quad \bar{\chi}_R) \begin{pmatrix} \rho_{c_2} \cos^2 \theta & -\sqrt{\rho_{c_1}\rho_{c_2}} \sin \theta \cos \theta \\ -\sqrt{\rho_{c_1}\rho_{c_2}} \sin \theta \cos \theta & \rho_{c_1} \sin^2 \theta \end{pmatrix} G_\mu^A T^A \gamma^\mu \begin{pmatrix} t_R \\ \chi_R \end{pmatrix} \\ & + \frac{g_{c_2}}{\rho_{c_1}\rho_{c_2} a(c_1, c_2)} (\bar{t}_R \quad \bar{\chi}_R) \begin{pmatrix} \rho_{c_1} \sin^2 \theta & \sqrt{\rho_{c_1}\rho_{c_2}} \sin \theta \cos \theta \\ \sqrt{\rho_{c_1}\rho_{c_2}} \sin \theta \cos \theta & \rho_{c_2} \cos^2 \theta \end{pmatrix} G_\mu^A T^A \gamma^\mu \begin{pmatrix} t_R \\ \chi_R \end{pmatrix}, \end{aligned} \quad (36)$$

where g_{c_i} is defined exactly as in Eq. (5) (i.e. as the coupling of the first KK gluon to a generic fermion with $(+, +)$ b.c.'s and localization parameter c_i). The above two matrices can be diagonalized by the same rotation matrix. Changing the RH chiral fermions basis to a new basis $t'_R \equiv \cos \alpha t_R + \sin \alpha \chi_R$ and $\chi'_R \equiv -\sin \alpha t_R + \cos \alpha \chi_R$, so that the fermion couplings to the first KK gluon are diagonal, we have the simple result

$$(\bar{t}'_R \quad \bar{\chi}'_R) \begin{pmatrix} g_{c_1} & 0 \\ 0 & g_{c_2} \end{pmatrix} G_\mu^A T^A \gamma^\mu \begin{pmatrix} t'_R \\ \chi'_R \end{pmatrix}, \quad (37)$$

with the mixing angle

$$\alpha = -\tan^{-1}(\sqrt{\rho_{c_1}/\rho_{c_2}} \tan \theta). \quad (38)$$

Effectively, t'_R and χ'_R behave like RH zero-modes of two non-mixing Dirac fermions with localization parameters c_1 and c_2 . They couple to the LH light fermion χ_L with 4D Dirac masses, $\sin \alpha m_d$ and $\cos \alpha m_d$, respectively, where m_d is given in Eq. (35). We notice, for future reference, that the normalization factor in Eq. (33) can be variously expressed as

$$a(c_1, c_2) = \frac{\cos^2 \theta \sec^2 \alpha}{\rho_{c_1}} = \frac{\sin^2 \theta \csc^2 \alpha}{\rho_{c_2}} = \frac{\sec^2 \alpha}{\rho_{c_1} + \tan^2 \alpha \rho_{c_2}}, \quad (39)$$

so that the wavefunction profiles of Eqs. (32) and (34) can be simply written in terms of the fundamental zero-mode wavefunctions of Eq. (2) as

$$\begin{aligned} h_1(y) &= \cos \alpha f_{c_1}(y), & h_2(y) &= \sin \alpha f_{c_2}(y), \\ k_1(y) &\approx \sin \alpha f_{c_1}(y), & k_2(y) &\approx -\cos \alpha f_{c_2}(y). \end{aligned} \quad (40)$$

The wavefunction of χ_L is obtained from χ_R using the equation of motion. Decomposing the 5D left-handed field as

$$\Psi_{1L}(x, y) = \frac{e^{\frac{3}{2}ky}}{\sqrt{L}} l_1(y) \chi_L(x) + \dots, \quad \Psi_{2L}(x, y) = \frac{e^{\frac{3}{2}ky}}{\sqrt{L}} l_2(y) \chi_L(x) + \dots, \quad (41)$$

and considering the region $c_{1,2} < -1/2$, we have

$$l_1(y) \approx -\frac{\sin \theta}{\sqrt{a(-c_2, -c_1)}} e^{(\frac{1}{2}+c_1)ky}, \quad l_2(y) = \frac{\cos \theta}{\sqrt{a(-c_2, -c_1)}} e^{(\frac{1}{2}+c_2)ky}, \quad (42)$$

where the normalization factors were defined in Eq. (33). The coupling of χ_L to the first KK gluon, which we call g_{χ_L} , can be calculated simply by substituting the wave function profiles $l_1(y)$ and $l_2(y)$ into Eq.(5) and summing them together. As one can see, for the parameter range of interest, $c_{1,2} < -1/2$, the LH part of the Dirac fermion is localized close to the UV brane. As a consequence, g_{χ_L} is suppressed compared to g_{c_1} and g_{c_2} . More importantly, it has the *opposite* sign to g_{c_1} and g_{c_2} , a fact that will be relevant in the following.

3.2 EWSB, Radion Stabilization and the Top Mass

It is now simple to study the low-energy theory that describes the light fermions, $Q_L = (t_L, b_L)$, t'_R , χ_L and χ'_R . The most important effects due to the heavy physics are the 4-fermion interactions that are induced by integrating out the KK gluons at tree-level. These lead to the breaking of the EW symmetry and the stabilization of the radion along the lines discussed in Section 2. The top mass can also be easily accommodated via a top seesaw. After Fierz rearrangement, the 4-fermion operators are

$$\frac{1}{M_{\text{KK}}^2} \left[g_{\chi_L \chi_R}^2 (\bar{\chi}_L \chi'_R) (\bar{\chi}'_R \chi_L) + g_{\chi_L t}^2 (\bar{\chi}_L t'_R) (\bar{t}'_R \chi_L) + g_{Q \chi_R}^2 (\bar{Q}_L \chi'_R) (\bar{\chi}'_R Q_L) + g_{Q t}^2 (\bar{Q}_L t'_R) (\bar{t}'_R Q_L) \right], \quad (43)$$

where M_{KK} is the KK gluon mass, and $g_{\chi_L \chi_R}^2 = g_{\chi_L} g_{c_2}$, $g_{\chi_L t}^2 = g_{\chi_L} g_{c_1}$, $g_{Q \chi_R}^2 = g_{c_Q} g_{c_2}$, $g_{Q t}^2 = g_{c_Q} g_{c_1}$. The analytical dependence of these coupling on L can be obtained from Eq. (10), with

$$g_5^2 \rightarrow g_{s,5}^2 + \left(\frac{Y_i}{2}\right) \left(\frac{Y_j}{2}\right) g_{Y,5}^2. \quad (44)$$

Here $g_{s,5}^2$ and $g_{Y,5}^2$ are the $SU(3)_C$ and $U(1)_Y$ 5D gauge couplings, respectively, and the Y_i 's are the appropriate hypercharges, with $Y_\chi = Y_{t_R} = 4/3$ and $Y_Q = 1/3$. There is no contribution

from the $SU(2)_L$ interactions since all terms in Eq. (43) involve the $SU(2)_L$ singlets t'_R or χ'_R . For $g_{Q_{XR}}^2$ and g_{Qt}^2 , Eqs. (7) and (8) can be used, since they apply for fermions localized near the IR brane. However, as mentioned at the end of the previous subsection, one finds that g_{χ_L} has the opposite sign to g_{c_1} and g_{c_2} , so that $g_{\chi_L \chi_R}^2$ and $g_{\chi_L t}^2$ are negative.⁹ Thus, KK gluon exchange in these channels is repulsive, and no singlet bound states can form. Bound states and condensation can only occur for $\overline{Q}_L \chi'_R$ and $\overline{Q}_L t'_R$.

In order to analyze the physics of EW symmetry breaking, we introduce two scalar $SU(2)_L$ doublets, H_1 and H_2 , with hypercharge $Y_H = -1$. In terms of these auxiliary scalar fields, the last two terms in Eq. (43) are rewritten as

$$\mathcal{L}_4 \supset g_{Q_{XR}} \overline{Q}_L H_1 \chi'_R + g_{Qt} \overline{Q}_L H_2 t'_R - M_{\text{KK}}^2 (H_1^\dagger H_1 + H_2^\dagger H_2), \quad (45)$$

which is understood to hold at the KK scale, M_{KK} . We do not write the four fermion operators involving χ_L since they do not lead to scalar bound states, nor condensation. At lower scales the scalar fields H_1 and H_2 become dynamical and, depending on the strength of their interactions with the fermions, their squared masses can become negative, thus triggering the condensation. The induced scalar kinetic terms, quartic couplings and mass renormalizations can be obtained by RG evolution. The RG equations receive contributions from the Yukawa couplings exhibited in Eq. (45), as well as from the gauge interactions and the induced quartic self-interactions. At lower energies, the Lagrangian, with kinetic terms understood, takes the form

$$\begin{aligned} \mathcal{L}_4 \supset & \bar{g}_{Q_{XR}} \overline{Q}_L H_1 \chi'_R + \bar{g}_{Qt} \overline{Q}_L H_2 t'_R - \bar{m}_{H_1}^2 H_1^\dagger H_1 - \bar{m}_{H_2}^2 H_2^\dagger H_2 \\ & - \frac{\bar{\lambda}}{2} [(H_1^\dagger H_1)^2 + (H_2^\dagger H_2)^2 + 2 H_1^\dagger H_1 H_2^\dagger H_2]. \end{aligned} \quad (46)$$

The bars indicate renormalized parameters with all fields canonically normalized, as in Eq. (16):

$$\bar{m}_i^2 = \frac{m_i^2}{\mathcal{Z}_i}, \quad \bar{\lambda} = \frac{32\pi^2}{N_c \log\left(\frac{M_{\text{KK}}^2}{\mu^2}\right)}, \quad \bar{g}_i = \bar{g} = \frac{4\pi}{\sqrt{N_c \log\left(\frac{M_{\text{KK}}^2}{\mu^2}\right)}}, \quad (47)$$

where the \mathcal{Z}_i 's are the scalar wavefunction renormalization constants induced at low-energies. Here only the effects of the Yukawa interactions are shown, and the m_i are given by Eqs. (13) replacing the appropriate Yukawa couplings. An improved analysis that takes into account

⁹For a fermion zero-mode with localization parameter $c_{\text{UV}} > 1/2$ (localized near the UV brane) interacting via KK gluon exchange with a second fermion with $c_{\text{IR}} < 1/2$ (localized near the IR brane), one has, for $kL \gg 1$, $g_{c_{\text{UV}}} g_{c_{\text{IR}}} \approx -g_5^2 k x_1^2 [f_2(c_{\text{IR}})/(kL) + 1/(4k^2 L^2)]$ with $f_2(c_{\text{IR}}) = (5 - 12c_{\text{IR}} + c_{\text{IR}}^2)/(4(3 - 2c_{\text{IR}})^2) > 0$.

the effects of the gauge and quartic couplings is straightforward. As will become clear in the following, in the case of interest to us the RG improved analysis is identical to the analysis done in Subsection 2.5.

To simplify our discussion, we consider the following region of parameter space: $c_Q \leq c_2 < c_1 < -1/2$,¹⁰ which leads to an ordering of 4-fermion coefficients: $g_{Q\chi R}^2 > g_{Qt}^2$ (with $g_{\chi L\chi R}^2$ and $g_{\chi Lt}^2$ small and negative). Furthermore, we consider the case with $g_{Q\chi R}$ slightly above the critical value G_c^2 of the NJL model [see Eq. (14)]. Due to the relaxation mechanism discussed in Subsection 2.4, generically we have g_{Qt} below the critical value unless c_1 is accidentally extremely close to c_Q . Hence the vacuum of the potential should have $\langle H_2 \rangle = 0$, and a nonzero VEV for H_1 . For this range of parameters, only H_1 plays a role in stabilizing the radion. The radion potential is simply given by Eq. (15), changing H to H_1 :

$$V(H_1, L) = \bar{m}_{H_1}^2(L) H_1^\dagger H_1 + \frac{\bar{\lambda}(L)}{2} (H_1^\dagger H_1)^2. \quad (48)$$

The analysis to determine the VEV's of H_1 and L is the same as in Subsection 2.3.

After the EW symmetry is broken by $\langle H_1 \rangle = v_{EW}$, t_L obtains a dynamical mass by marrying with the χ'_R field. Including the Dirac mass of the light KK mode χ , the mass terms take the form $\bar{g}_{Q\chi R} \langle H_1 \rangle \bar{t}_L \chi'_R + \sin\alpha m_d \bar{\chi}_L t'_R + \cos\alpha m_d \bar{\chi}_L \chi'_R + \text{h.c.}$, which can be recognized as the “top seesaw” structure. We find it more useful to consider the fermion mass matrix in the original KK basis (t_R, χ_R) , rather than in the rotated basis (t'_R, χ'_R) that was useful in analyzing the physics of condensation. It reads

$$(\bar{t}_L \quad \bar{\chi}_L) \begin{pmatrix} -\sin\alpha \bar{g}_{Q\chi R} \langle H_1 \rangle & \cos\alpha \bar{g}_{Q\chi R} \langle H_1 \rangle \\ 0 & m_d \end{pmatrix} \begin{pmatrix} t_R \\ \chi_R \end{pmatrix}. \quad (49)$$

In the limit that the Dirac mass is large, $m_d \gg \bar{g}_{Q\chi R} \langle H_1 \rangle$, the physical top quark mass is

$$m_t^2 \approx \sin^2\alpha (\bar{g}_{Q\chi R} \langle H_1 \rangle)^2, \quad (50)$$

while the mass of the extra colored physical quark field χ is

$$m_\chi^2 \approx m_d^2 + \cos^2\alpha (\bar{g}_{Q\chi R} \langle H_1 \rangle)^2. \quad (51)$$

In our model, we have 5 free parameters: g_5 , c_Q , c_1 , c_2 and θ to fit three observed quantities: α_s , v_{EW} and m_t . Since only g_5 , c_Q and c_2 enter the potential of H_1 and L , through $g_{Q\chi R}^2 = g_{c_Q} g_{c_2}$,

¹⁰We choose $c_2 < c_1$ without loss of generality, since we can always relabel Ψ_1 and Ψ_2 to have a more negative Dirac mass for Ψ_2 . The assumption that c_Q is more negative than the other localization parameters ensures that the condensed bound state is a doublet under the $SU(2)_L$ gauge group.

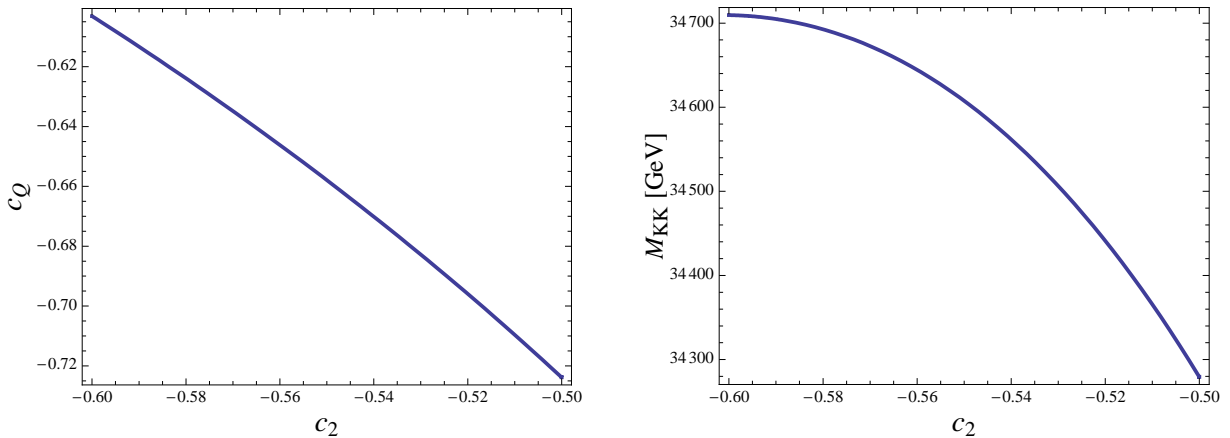


Figure 4: Left panel: the curve corresponding to $v_{\text{EW}} = 174$ GeV in the c_2 - c_Q plane. Right panel: the mass of the first KK gauge boson as a function of c_2 (the corresponding c_Q on the curve of the left panel for a given c_2 is used).

we determine their values first by fitting v_{EW} and α_s . By minimizing the potential w.r.t. H_1 and L , we show in Fig. 4 the curve in the c_Q - c_2 plane corresponding to $\langle H_1 \rangle = v_{\text{EW}} = 174$ GeV. The mass of the first KK gluon M_{KK} is around 35 TeV, as can be seen on the right panel of Fig. 4, and this result is stable against variations of the localization parameters that reproduce $v_{\text{EW}} = 174$ GeV, and insensitive to the precise value of the curvature k . In these figures, $k = 2 \times 10^{17}$ GeV and $\mu = v_{\text{EW}}$ are used. We also use the effective coupling $g_5 \sqrt{k} = 5.12$, which is defined in Eq. (44) and calculated at the $M_{\text{KK}} \approx 35$ TeV scale by assuming the mass of the additional χ field to be around 2 TeV (see Subsection 4.2). The lower value of $c_2 \approx -0.60$ guarantees $c_Q < c_2$.

Having determined c_Q as a function of c_2 from v_{EW} , we are left with three parameters c_1 , c_2 and θ to fit the top quark mass. Substituting $m_t = 172.4$ GeV [31] and the RG improved value of $\bar{g}_{Q\chi R} \langle H_1 \rangle = 375$ GeV as discussed in Section 2.5 into Eq. (50), we see that $\sin \alpha \approx 0.46$. Then θ is determined as a function of c_1 and c_2 from Eq. (38) as $\tan \theta = -\tan \alpha \sqrt{\rho_{c_2}/\rho_{c_1}}$. Finally, only two free parameters, c_1 and c_2 , are left to determine the spectrum of other particles in our model such as the heavy top quark, which is around 2 TeV to be compatible with electroweak precision observables, as discussed in Section 4.2.

The second doublet H_2 is heavier than the Higgs boson h unless one fine-tunes g_{Qt}^2 to be extremely close to $g_{Q\chi R}^2$ so that it is also close to G_c^2 . For a typical c_1 , m_{H_2} is around 10 TeV.

3.3 Light Fermion Masses

Since the 5D theory is non-renormalizable, 5D local 4-fermion operators are anticipated to exist in the bulk, e.g.

$$\mathcal{L}_5 \supset \frac{d_\xi}{\Lambda^3} (\bar{\Psi}_{\xi_L} \Psi_{\xi_R}) (\bar{\Psi}_{Q_L} \Psi_2) + \text{h.c.} + \dots, \quad (52)$$

where d_ξ is an unknown dimensionless coefficient, and Ψ_{ξ_L} and Ψ_{ξ_R} are 5D spinors with their zero modes ξ_L and ξ_R representing SM fermions (one of them is an $SU(2)_L$ doublet, the other one a singlet). Those operators involving only the top and Ψ_2 fields can be added to the 4-fermion interactions induced by gluon exchange discussed before. However, as argued in Appendix A, these contributions are expected to be a small correction compared to the gluon-induced ones. Hence, our analysis of the dynamical breaking of the EW symmetry, with the concomitant stabilization of the radion field, and the generation of the top mass is not expected to be affected much by such effects. Nevertheless, the local higher-dimension operators involving the other SM fermion fields would be responsible, in the present scenario, for giving rise to the remaining Yukawa interactions.¹¹ Indeed, after integrating out the fifth dimension, Eq. (52) induces the following 4-fermion interactions in the 4D effective theory:

$$\mathcal{L}_4 \supset \frac{d_\xi}{(\Lambda L) \tilde{\Lambda}^2} f_{\xi_L \xi_R \chi'_R Q_L} (\bar{\xi}_L \xi_R) (\bar{\chi}'_R Q_L) + \text{h.c.} + \dots, \quad (53)$$

where $\tilde{\Lambda} = \Lambda e^{-kL}$ is the warped down cutoff, ξ_L and ξ_R are the standard model fermions (zero modes) and

$$\begin{aligned} f_{\xi_L \xi_R \chi'_R Q_L} &= \frac{1}{L} \int_0^L dy e^{-2k(L-y)} f_{\xi_L}(y) f_{\xi_R}(y) f_{Q_L}(y) [\cos \alpha k_2(y) - \sin \alpha h_2(y)] \\ &= -\frac{\sqrt{\rho_{c_{\xi_L}} \rho_{c_{\xi_R}} \rho_{c_{Q_L}} \rho_{c_2}}}{e^{2kL} \rho_{-\frac{1}{2}(3-c_{\xi_L}-c_{\xi_R}-c_{Q_L}-c_2)}}, \end{aligned}$$

with $f_i(y)$ and ρ_{c_i} as defined in Eqs. (2) and (3), respectively, while $h_2(y)$ and $k_2(y)$ are given in Eq. (40).

In order to see how the Yukawa couplings between the ξ fields and the Higgs arise consider an operator of the form Eq. (53) together with the $(g_{Q_{XR}}^2/M_{\text{KK}}^2)(\bar{Q}_L \chi'_R)(\bar{\chi}'_R Q_L)$ operator in Eq. (43). In terms of the bilinears $B_1 = \bar{\xi}_L \xi_R$ and $B_2 = \bar{Q}_L \chi'_R$, we simply have

$$\frac{d_\xi}{(\Lambda L) \tilde{\Lambda}^2} f_{\xi_L \xi_R \chi'_R Q_L} B_1 B_2^\dagger + \frac{g_{Q_{XR}}^2}{M_{\text{KK}}^2} B_2 B_2^\dagger = \frac{g_1^2}{M_{\text{KK}}^2} \tilde{B}_1 \tilde{B}_1^\dagger + \frac{g_2^2}{M_{\text{KK}}^2} \tilde{B}_2 \tilde{B}_2^\dagger, \quad (54)$$

¹¹Notice that KK gluon exchange does not induce “non-diagonal” operators of the form Eq. (52).

where $\tilde{B}_1 = \cos\gamma B_1 + \sin\gamma B_2$ and $\tilde{B}_2 = -\sin\gamma B_1 + \cos\gamma B_2$ are linear combinations that “diagonalize” the above 4-fermion interactions, and g_1^2/M_{KK}^2 , g_2^2/M_{KK}^2 are the corresponding eigenvalues. To the extent that $d_\xi/(\tilde{\Lambda}^2\Lambda L) f_{\xi_L\xi_R\chi'_R Q_L} \ll g_{Q_{XR}}^2/M_{\text{KK}}^2$, we have $g_1^2 \ll g_2^2 \approx g_{Q_{XR}}^2$ while the mixing angle is given by $\gamma \approx [d_\xi/(g_{Q_{XR}}^2\Lambda L)](M_{\text{KK}}^2/\tilde{\Lambda}^2) f_{\xi_L\xi_R\chi'_R Q_L}$. Only the second 4-fermion interaction on the r.h.s. of Eq. (54) is sufficiently strong to lead to a condensate, exactly along the lines discussed in previous sections. Describing this process by the introduction of an auxiliary scalar field H_1 , we end up with a Yukawa interaction of the form $\bar{g}_{Q_{XR}}\tilde{B}_2 H_1 = -\bar{g}_{Q_{XR}}\sin\gamma\bar{\xi}_L\xi_R H_1 + \bar{g}_{Q_{XR}}\cos\gamma\bar{Q}_L\chi'_R H_1$, where $\bar{g}_{Q_{XR}}$ is the running Yukawa coupling at a scale μ , as discussed in Subsection 2.5. Therefore, the ξ Yukawa coupling is

$$y_\xi = \frac{\bar{g}_{Q_{XR}}}{g_{Q_{XR}}^2} \frac{d_\xi M_{\text{KK}}^2}{(\Lambda L)\tilde{\Lambda}^2} f_{\xi_L\xi_R\chi'_R Q_L} \approx \frac{N_c\bar{g}_{Q_{XR}}}{8\pi^2} \frac{d_\xi M_{\text{KK}}^2}{(\Lambda L)\tilde{\Lambda}^2} f_{\xi_L\xi_R\chi'_R Q_L}, \quad (55)$$

where in the second equality we used $g_{Q_{XR}}^2 \approx 8\pi^2/N_c$. This expression has a simple interpretation as a one-loop diagram obtained by an insertion of the operator Eq. (53), where the $\bar{\chi}'_R Q_L$ lines are closed with the Yukawa interaction $\bar{g}_{Q_{XR}}\bar{Q}_L H_1\chi'_R$ discussed in Eq. (46). This one-loop diagram is quadratically divergent, and should be cutoff at the scale M_{KK} . Up to order one factors this gives rise to a Yukawa coupling of the order of Eq. (55). Notice that the fact that the one-loop integral is dominated by the M_{KK} scale suggests evaluation of $\bar{g}_{Q_{XR}}$ at $\mu \sim M_{\text{KK}}$. Nevertheless, even at lower scales, $\bar{g}_{Q_{XR}}/g_{Q_{XR}} \approx (375/174)/\sqrt{8\pi^2/N_c} \approx 2/5$ [see Fig. 3] so that no significant changes of the previous estimate arising from these details are expected. Notice also that operators similar to Eq. (52) but involving Ψ_1 instead of Ψ_2 do not contribute to the Yukawa coupling.

It is useful to have approximate expressions for the above Yukawa couplings, taking into account the fact that Q_L and χ'_R are localized close to the IR brane (since these fields are assumed to have the strongest interactions with the KK gluons, thus triggering EWSB by a bifermion condensate). For light SM fermions ξ localized near the UV brane, we have

$$y_{\text{light}} \approx \frac{N_c\bar{g}_{Q_{XR}}}{8\pi^2} \frac{d_\xi M_{\text{KK}}^2}{(\Lambda L)\tilde{\Lambda}^2} k_L \frac{\sqrt{(1-2c_Q)(1-2c_2)(1-2c_{\xi_L})(1-2c_{\xi_R})}}{4-c_Q-c_2-c_{\xi_L}-c_{\xi_R}} e^{(1-c_{\xi_L}-c_{\xi_R})kL}, \quad (56)$$

where, as discussed in the next section, $c_Q \sim -2/3$, $c_2 \sim -1/2$. In order to estimate the unknown coefficient d_ξ we resort to NDA which, as shown at the end of Appendix A, gives $d_\xi^{\text{NDA}} \sim 24\pi^3/n$, where $n \lesssim 45$. Taking also $\Lambda \sim 10k$ and $M_{\text{KK}} = 2.45k$, the c -independent factor in Eq. (56) times $v = 174$ GeV evaluates to ~ 12 GeV/ n , which shows that the light fermion masses can be accommodated by an appropriate choice of $c_{\xi_L}, c_{\xi_R} > 1/2$.

For the bottom quark, which has $c_{\xi_L} = c_Q$ [the localization parameter for the (t_L, b_L) doublet], we need to take $c_{\xi_R} \equiv c_{b_R} < 1/2$, in which case

$$y_{\text{bottom}} \approx \frac{N_c \bar{g}_{Q\chi R}}{8\pi^2} \frac{d_b M_{\text{KK}}^2 v_{\text{EW}}}{(\Lambda L) \tilde{\Lambda}^2} kL \frac{(1 - 2c_Q) \sqrt{(1 - 2c_2)(1 - 2c_{b_R})}}{4 - 2c_Q - c_2 - c_{b_R}}. \quad (57)$$

For $c_Q \sim -2/3$, $c_2 \sim -1/2$ and, for example, $c_{b_R} = 0$, with the other parameters as above, this leads to a mass $m_b \sim 7 \text{ GeV}/n$. Given the uncertainties in the estimate of the unknown coefficient d_b , we conclude that it is not implausible that the bottom mass also arises from the above 4-fermion interactions.

4 Phenomenology

Our model predicts two new particles beyond the SM model, besides a heavy Higgs boson h with a mass around 500 GeV. They are a light radion field at the GeV scale and an extra colored heavy fermion χ with a mass in the TeV range. We will study constraints on new particle masses due to LEP bounds and electroweak precision observables, and discuss their phenomenological consequences in this scenario in turn.

4.1 The Radion

At tree-level in the 5D theory, the radion-dependent terms arise from the 5D Einstein-Hilbert action. The corresponding low-energy 4D action, with a canonically normalized radion reads [32]

$$S = \frac{M_5^3}{k} \int d^4x \sqrt{-g} \left(1 - \frac{\phi^2}{F^2} \right) \mathcal{R}_4 + \frac{1}{2} \int d^4x \sqrt{-g} \left\{ \partial_\mu \phi \partial^\mu \phi - V(H_1, -k^{-1} \ln \phi/F) \right\}, \quad (58)$$

where $\phi(x) \equiv F e^{-kT(x)}$ with $\langle T \rangle = L$ and $F = \sqrt{12M_5^3/k}$. Since the 4D Planck mass is $M_P^2 \approx M_5^3/k \sim (2 \times 10^{18} \text{ GeV})^2$, we have $F \approx 2\sqrt{3}M_P \approx 6.9 \times 10^{18} \text{ GeV}$. Unless otherwise specified, we take $M_5 \sim 10^{18} \text{ GeV}$ and $k = 2 \times 10^{17} \text{ GeV}$. Eq. (58) also contains the Higgs-radion potential of Eq. (48). As explained in previous sections, this determines dynamically $\langle H_1 \rangle = v_{\text{EW}}$ and $\langle T \rangle = L$. Writing $H_1 = v_{\text{EW}} + \frac{1}{\sqrt{2}}h$ and $\phi = \tilde{F} + \varphi$, with $\tilde{F} = F e^{-kL}$, Eq. (48) leads to the Higgs/radion mass matrix:

$$\frac{1}{2} \begin{pmatrix} h & \varphi/\tilde{F} \end{pmatrix} \begin{pmatrix} -2\bar{m}_{H_1}^2(l) & \sqrt{2}\bar{m}_{H_1}^2(l)v'_{\text{EW}}(l) \\ \sqrt{2}\bar{m}_{H_1}^2(l)v'_{\text{EW}}(l) & -4\bar{m}_{H_1}^2(l)v'_{\text{EW}}(l)^2 + \frac{1}{2} [\bar{m}_{H_1}^2(l)v_{\text{EW}}(l)^2]'' \end{pmatrix} \begin{pmatrix} h \\ \varphi/\tilde{F} \end{pmatrix},$$

where we used $v_{\text{EW}}^2 = -\bar{m}_{H_1}^2/\bar{\lambda}$, defined $l \equiv kL$, and it is understood that all the entries are evaluated at the minimum of the potential, $l_{\text{min}} = kL_{\text{min}}$ [see Eq. (23)]. We see that, in general, there is mass mixing between the radion and the Higgs boson. However, since $\langle\phi\rangle = \tilde{F} \gg v_{\text{EW}}$, the mixing angle is extremely small. For the benchmark point discussed in Section 3, with $c_2 = -0.535$ and $c_Q = -0.675$, we have $\langle\phi\rangle = 490$ TeV, and the mixing angle is approximately 1.3×10^{-5} which can be neglected.¹² Therefore, the Higgs boson mass m_h is still as determined in the improved RG analysis of Subsection 2.5, around 500 GeV. The mass of the radion is $m_\varphi^2 \approx \frac{1}{2} [\bar{m}_{H_1}^2(l)v_{\text{EW}}(l)^2]'' / \tilde{F}^2 \approx (0.4 \text{ GeV})^2$, where the terms proportional to $v'_{\text{EW}}(l)$ are subdominant and can be neglected. Note that the radion mass is of order $v_{\text{EW}}^2/\tilde{F}$. The denominator \tilde{F} is related to the spontaneously broken conformal symmetry; the numerator is related to the explicit breaking of the conformal symmetry, since the electroweak scale is different from zero only when the localization parameters are away from the conformally invariant limit $c_Q = c_2 = 1/2$.

To have a better estimate of the allowed radion masses in our model, we vary the 5D curvature in the window $k \in (1 \times 10^{17}, 2 \times 10^{18})$ GeV, and adjust M_5 so as to keep the 4D Planck mass M_P unchanged. For each k , we first determine the allowed values of c_Q and c_2 to have the correct v_{EW} , and then calculate the radion and Higgs boson masses. Since $(g_{Q\chi R}^2 - G_c^2)/G_c^2 \ll 1$ at the minimum of the potential, the mass of the radion takes the approximate form

$$m_\varphi \approx \frac{3 x_1 \bar{f}_2 k M_{\text{KK}}}{64 \pi^3 \log^2 \left(\frac{x_1 k}{M_{\text{KK}}} \right) \log^{\frac{1}{2}} \left(\frac{M_{\text{KK}}}{\mu} \right) M_P} \approx \frac{k}{M_P} (4 \text{ GeV}) , \quad (59)$$

where \bar{f}_2 was defined in Eq. (22) and $x_1 \approx 2.45$. The mass of the Higgs boson and the mass of the first KK gluon do not vary much when k is varied, and they are still around 500 GeV and 35 TeV respectively. In the left panel of Fig. 5, the radion mass is shown as a function of k . As can be seen, m_φ is a linear function of k and is around a few GeV in the above window for k . In the right panel of Fig. 5, the radion VEV $\langle\phi\rangle = \tilde{F}$ is shown as a function of k , and, for $k/M_P < 0.5$, is of order a few hundred TeV.

The radion field couples to ordinary matter via the energy-momentum tensor, and its couplings are inversely proportional to the scale invariance (spontaneous) symmetry breaking scale.

¹²Higgs/curvature mixing as first discussed in [33] would arise from a higher-dimension bulk operator in the 5D theory that involves four fermion fields and the Ricci curvature scalar, where the fermions bilinears are replaced by the effective Higgs degrees of freedom at energies below the KK scale. The resulting coefficient in the 4D theory is therefore expected to be suppressed at least by order $(k/\Lambda)(M_{\text{KK}}/\tilde{\Lambda})^4$, which makes it unlikely to be relevant for phenomenology.

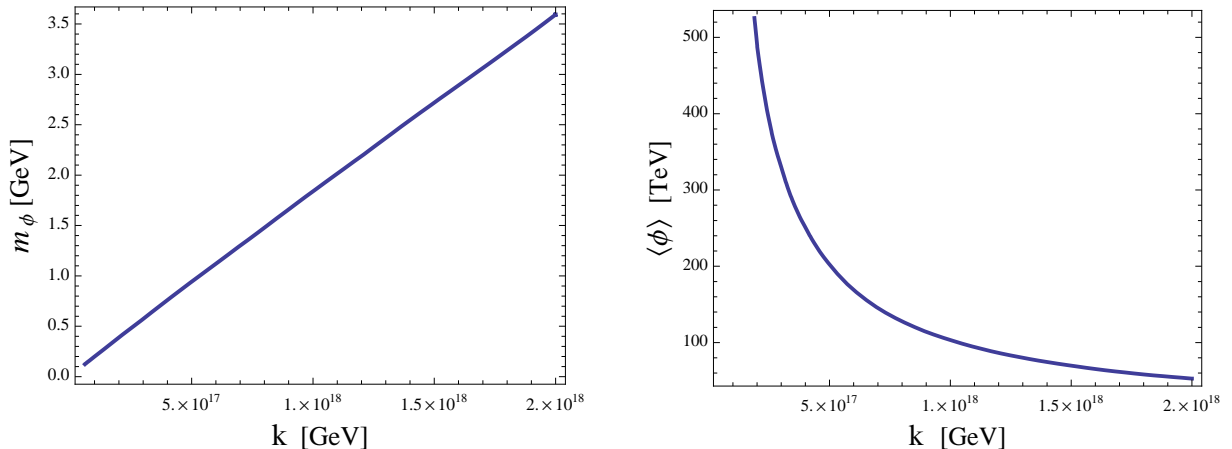


Figure 5: Left panel: the radion mass as a function of k . Right panel: the radion VEV $\langle\phi\rangle$ as a function of k .

In more detail [34],

$$\mathcal{L}_{int} = \frac{\phi}{\langle\phi\rangle} \left[\sum_{\psi} F_{c_{\psi}} m_{\psi} \bar{\psi} \psi + M_Z^2 Z^{\mu} Z_{\mu} + 2M_W^2 W^{+\mu} W_{-\mu} + \frac{\beta(g_s)}{2g_s} G^{a\mu\nu} G_{a\mu\nu} + \frac{\beta(e)}{2e} F^{\mu\nu} F_{\mu\nu} \right],$$

where $F_{c_{\psi}}$ is a function that depends on the fermion localization parameter, and $\beta(g_s)$ and $\beta(e)$ are the QCD and QED beta functions, taking all fermions lighter than the radion into account. LEP imposes bounds on the couplings of a light scalar to Z gauge bosons [35]. For the radion, these couplings are controlled by the ratio $v_{EW}/\langle\phi\rangle$, which in our case is a few $\times 10^{-4}$. This is below the current LEP upper bound on this ratio, which is about 10^{-1} .

4.2 Electroweak Precision Constraints and Spectrum

The oblique parameters S and T constrain the remaining two model parameters c_1 and c_2 (c_Q has already been determined by v_{EW} , θ is determined by m_t , and g_5 is determined by α_s). The U parameter in our model is much smaller than the S and T parameters, and is neglected in the following. In Appendix B, we give the formulas for ΔT and ΔS in our model, defined as the deviations of T and S from the standard model with a Higgs boson mass of 117 GeV. The dominant contribution to ΔS comes from the heavy Higgs of mass 450-500 GeV. The heavy fermions give a smaller contribution, and we have $\Delta S \approx 0.08$ for a wide range of choices of c_1 and c_2 . A two-parameter fit to the EW data with a reference mass of $m_h = 117$ GeV requires

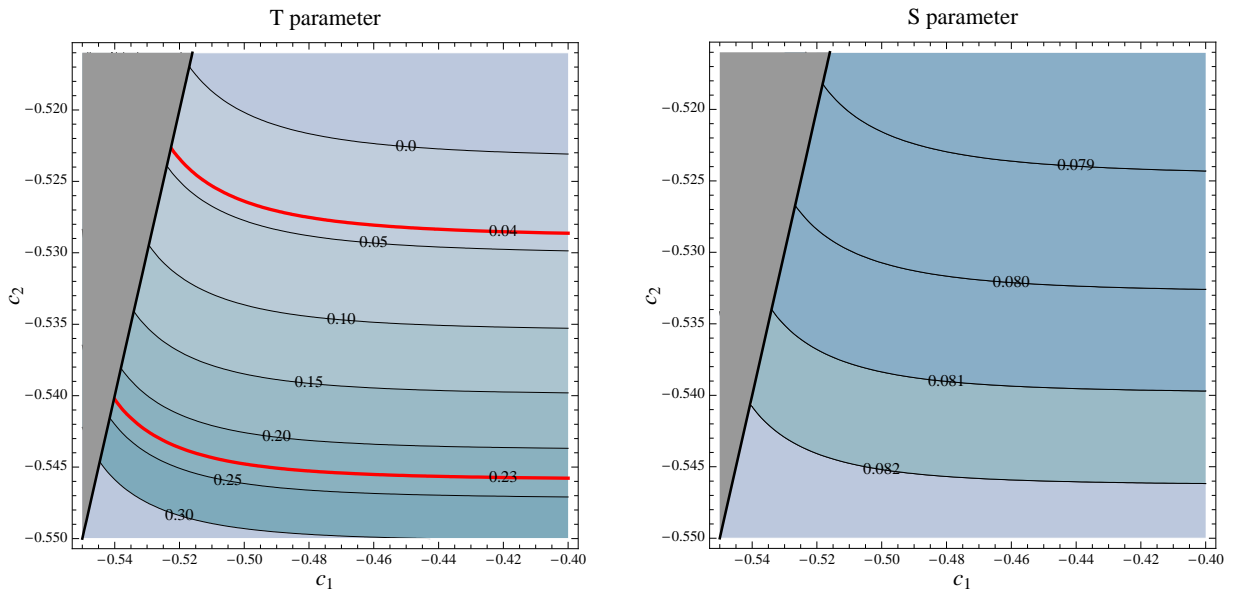


Figure 6: Left panel: curves of constant ΔT in the c_1 - c_2 plane. The two thick (red) lines demarcate the allowed region at the 95% CL. In this analysis we assumed $c_1 > c_2$ (see footnote 10), and therefore we show the complementary region in gray in the plots. Right panel: curves of constant ΔS in the c_1 - c_2 plane, showing that the region in the left panel has $\Delta S \approx 0.08$.

$0.04 < \Delta T < 0.23$ for $\Delta S = 0.08$, at the 95% CL.¹³ In Fig. 6, we show the allowed region of parameter space that satisfies the electroweak constraints. We impose $c_1 < c_2$, as discussed in Subsection 3.2. We also use $m_h = 475$ GeV and $\bar{g}_{Q\chi_R}\langle H_1 \rangle = 375$ GeV as described in Section 2.5. The left panel of Fig. 6 shows a contour plot of the T parameter as a function of c_1 and c_2 . The curves of constant ΔT are most sensitive to c_2 and are only mildly dependent on c_1 . This is because, for fixed $\bar{g}_{Q\chi_R}\langle H_1 \rangle$, the Dirac mass m_d controls the mixing of the left-handed top quark with the fermion $SU(2)_L$ singlet –which dominantly determines the contribution to ΔT from the fermion loops– and m_d is mainly controlled by c_2 . Since the 475 GeV Higgs boson contributes ~ -0.2 to ΔT , a positive and non-negligible contribution from fermion loops is necessary to bring the T parameter back to the experimentally allowed region. Therefore, there is an upper bound on the Dirac mass m_d (via an upper limit on c_2). In the right panel of Fig. 6, we show a contour plot for the S parameter as a function of c_1 and c_2 , showing that indeed $\Delta S \approx 0.08$ in the region of interest (the 475 GeV Higgs boson contributes ~ 0.07 to ΔS

¹³The fit does not include low-energy data, but the latest measurements of $m_W = 80.432 \pm 0.039$ GeV and $m_t = 172.4 \pm 1.2$ GeV at the Tevatron are included in the fit. We thank Jens Erler for kindly providing the fit results, which we have reproduced with good agreement using the code in [36].

while χ contributes ~ 0.01). There are also tree-level contributions to the S and T parameters that arise when the heavy KK gauge bosons are integrated out, but for $M_{\text{KK}} \approx 35$ TeV these are one order of magnitude smaller than the fermion and Higgs boson loop-level contributions, and are not included in the plots.

Notice that in our setup the (t_L, b_L) $SU(2)_L$ doublet is extremely localized towards the IR brane, thus triggering EWSB through the condensate. As mentioned above, the KK scale is dynamically set to be about $M_{\text{KK}} \approx 35$ TeV, which corresponds to $\tilde{k} \equiv k e^{-kL} \approx 14$ TeV. This high scale allows localizing the light families close to the UV brane –so that the fermion mass hierarchies arise from wavefunction localization effects– without inducing large anomalous contributions to the $Z\bar{b}_L b_L$ coupling due to mixing with the heavy KK gauge bosons. In fact, assuming that the light fermions are localized near the UV brane, we have ¹⁴

$$\frac{\delta g_{b_L}^{\text{tree}}}{g_{b_L}} \approx -\frac{e^2}{s_W^2 c_W^2} \frac{v_{\text{EW}}^2}{\tilde{k}^2} \frac{(4c_Q^2 - 16c_Q + 7)kL}{8(4c_Q^2 - 16c_Q + 15)} \xrightarrow{c_Q \rightarrow -\infty} -\frac{e^2}{s_W^2 c_W^2} \frac{v_{\text{EW}}^2}{\tilde{k}^2} \frac{kL}{8}. \quad (60)$$

For $v_{\text{EW}} = 174$ GeV, $\tilde{k} \approx 14$ TeV and $kL \approx 30$, one finds $\delta g_{b_L}^{\text{tree}}/g_{b_L} \approx -3 \times 10^{-4}$. There is also a loop-level correction to the $Z\bar{b}_L b_L$ vertex induced by the vector-like quark χ through its mixing with the top quark. In the limit that χ is much heavier than the top quark, we have [37]

$$\delta g_{b_L}^{\text{loop}} \approx \frac{e^2}{64\pi^2 s_W^2 M_W^2} \frac{(\bar{g}_{Q\chi R} \cos \alpha \langle H \rangle)^4}{m_\chi^2} \left[1 + 2 \frac{m_t^2}{(\bar{g}_{Q\chi R} \cos \alpha \langle H \rangle)^2} \left(\log \frac{m_\chi^2}{m_t^2} - 1 \right) \right], \quad (61)$$

which gives¹⁵ $\delta g_{b_L}^{\text{loop}}/g_{b_L} \approx -2.4 \times 10^{-3}$ for $m_\chi = 2$ TeV (see below), $\bar{g}_{Q\chi R} \langle H \rangle = 375$ GeV and $\alpha = 0.48$. Adding the tree-level and loop-level contributions, one has $\delta g_{b_L}/g_{b_L} \approx -2.7 \times 10^{-4}$, which is comparable to the current experimental bound. Moreover, the dominant contributions to ΔT and δg_{b_L} depend on the same underlying model parameters (but are essentially uncorrelated with S). Nevertheless, we have checked that the 95% CL ellipsoid resulting from a simultaneous fit to S , T and δg_{b_L} , using the code in [36], results in essentially the same allowed range in ΔT as discussed above. Therefore, the additional constraints from δg_{b_L} turn out to be very mild.

The constraints from EW observables discussed above in the c_1 - c_2 plane allow us to constrain the mass of the vector-like fermion χ . For c_2 less than but not too close to c_1 , so that

¹⁴We assume that the EW breaking VEV is effectively localized on the IR brane. A more detailed analysis that takes into account the fact that the fermionic Higgs constituents have profiles that extend into the extra dimension most likely will reduce this estimate even further.

¹⁵We thank José Santiago for pointing out a missing factor in Eq. (61) of an earlier version.

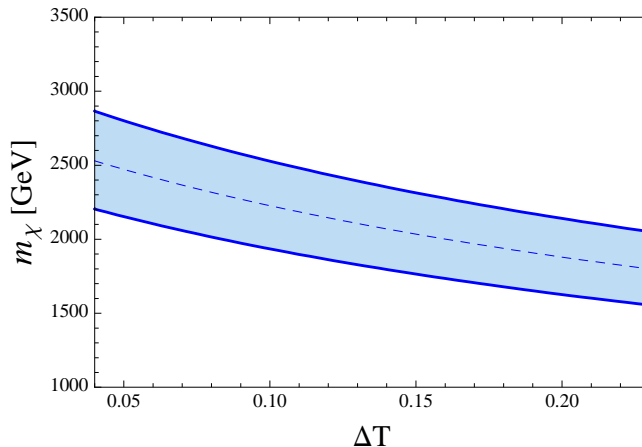


Figure 7: The mass of the χ field as a function of ΔT . The dashed line is for the central value of $\bar{g}_{Q_{XR}}\langle H_1 \rangle = 375$ GeV, while the thick lines are for 350 GeV and 400 GeV, respectively [adjusting the angle α to keep m_t fixed, see Eq. (49)]. The variation of the Higgs mass in the 450–500 GeV range changes the curves only slightly.

$e^{-(c_1 - c_2)kL} \ll 1$, we obtain an approximate expression for m_χ , which is almost independent of c_1 :

$$m_\chi \approx \sqrt{4c_2^2 - 1} \sec \alpha e^{(c_2+1/2)kL} \tilde{k}, \quad (62)$$

Recall that $\alpha \approx \arcsin m_t / (\bar{g}_{Q_{XR}}\langle H \rangle) \approx 0.48$ for $\bar{g}_{Q_{XR}}\langle H \rangle = 375$ GeV. This approximate formula for m_χ holds for $m_d \gg \bar{g}_{Q_{XR}}\langle H_1 \rangle$ and is within 5% of the exact value. In Fig. 7, we show the mass of the χ field as a function of ΔT . The contribution to ΔT due to the χ fermion depends on the Dirac mass m_d and the mixing with the top quark which is governed by $\bar{g}_{Q_{XR}}\langle H_1 \rangle$ [see Eq. (49)]. The dashed line corresponds to the central value $\bar{g}_{Q_{XR}}\langle H_1 \rangle = 375$ GeV. The band corresponds to the variation of $\bar{g}_{Q_{XR}}\langle H_1 \rangle$ between 350 GeV and 400 GeV. We adjust the angle α to reproduce the top mass m_t , and also take into account its effect, through θ , on m_d [see Eqs. (35) and (38), although we do not use the approximate expression (35) but instead solve the exact eigenvalue equation to obtain m_d]. We see that the electroweak constraints determine m_χ to be between 1.6 and 2.9 TeV.

4.3 Collider Phenomenology

In this section, we explore the prospects for discovery of the heavy Higgs boson and the new colored fermion at the LHC. After diagonalization of Eq. (49), we obtain the top and heavy fermion mass eigenstates with their masses given by Eqs. (50) and (51). As discussed above,

our model has definite predictions for their masses. To simplify the notation, from now on we shall denote the fermion mass eigenstates as t and χ . The relevant interactions of h and χ with other particles in unitary gauge are

$$\begin{aligned}
\mathcal{L}_{\text{int}} \supset & \frac{e}{s_W c_W} Z_\mu \left[\bar{t}_L \gamma^\mu \left(\frac{1}{2} c_{\beta_L}^2 - s_W^2 Q_t \right) t_L + \bar{\chi}_L \gamma^\mu \left(\frac{1}{2} s_{\beta_L}^2 - s_W^2 Q_\chi \right) \chi_L \right. \\
& + \bar{\chi}_L \gamma^\mu \left(\frac{1}{2} s_{\beta_L} c_{\beta_L} \right) t_L + \bar{t}_L \gamma^\mu \left(\frac{1}{2} s_{\beta_L} c_{\beta_L} \right) \chi_L - s_W^2 Q_t \bar{t}_R \gamma^\mu t_R - s_W^2 Q_\chi \bar{\chi}_R \gamma^\mu \chi_R \left. \right] \\
& + \frac{e}{\sqrt{2} s_W} W_\mu^+ (c_{\beta_L} \bar{t}_L \gamma^\mu b_L + s_{\beta_L} \bar{\chi}_L \gamma^\mu b_L) + \frac{e}{\sqrt{2} s_W} W_\mu^- (c_{\beta_L} \bar{b}_L \gamma^\mu t_L + s_{\beta_L} \bar{b}_L \gamma^\mu \chi_L) \\
& + \frac{m_t}{\sqrt{2} v_{\text{EW}} s_\alpha} h (c_{\beta_L} s_{\beta_R - \alpha} \bar{t}_L t_R + s_{\beta_L} c_{\beta_R - \alpha} \bar{\chi}_L \chi_R + c_{\beta_L} c_{\beta_R - \alpha} \bar{t}_L \chi_R + s_{\beta_L} s_{\beta_R - \alpha} \bar{\chi}_L t_R + \text{h.c.}) ,
\end{aligned} \tag{63}$$

where $Q_t = Q_\chi = 2/3$ are the top and χ electric charges and $s_{\beta_{L,R}} \equiv \sin \beta_{L,R}$ with $\beta_{L,R}$ the left- and right-handed mixing angles obtained from diagonalization of the fermion mass matrix, Eq. (49). The exact formula for β_L is given in Eq. (74), but for $m_\chi \gg \bar{g}_{Q\chi R} \langle H_1 \rangle$ we have the simple result $\beta_L \approx (m_t/m_\chi) \cot \alpha$. For $\alpha = 0.48$, $\bar{g}_{Q\chi R} \langle H_1 \rangle = 375$ GeV and $m_\chi = 2$ TeV we have $\beta_L \approx 0.16$. The right-handed mixing angle is $\beta_R \approx 0$ for the same set of parameters. We note here that deviations of the top Yukawa coupling from its SM value are of order m_t^2/m_χ^2 , which, for the above parameters, results in a decrease of about 2%.

The Higgs boson in our model has a mass around 475 GeV, and is heavy enough to decay into a pair of W gauge bosons, Z gauge bosons or top quarks. Taking the running of fermion masses into account, a SM Higgs of mass 475 GeV has a total width of $\Gamma_h^{\text{total}} \approx 56.6$ GeV, and the branching ratios of the three main decay channels are $Br(h \rightarrow \bar{t}t) \approx 19.5\%$, $Br(h \rightarrow W^+W^-) \approx 54.5\%$ and $Br(h \rightarrow ZZ) \approx 26.0\%$, respectively [38, 39]. In our model, the changes of those branching ratios from their SM values are of order m_t^2/m_χ^2 due to the deviation of the top Yukawa coupling from its SM value, and are negligible. Unlike a light Higgs, a heavy Higgs boson mainly decays to gauge bosons due to the enhancement of its decays into the longitudinal components of the gauge bosons as its mass gets larger.

At the LHC, the dominant production of the Higgs boson is through gluon fusion. The new quark χ , is too heavy and has too small a coupling to the Higgs boson (its mass gets only a small contribution from the EWSB) to contribute appreciably to the Higgs boson production. Compared to the Higgs boson in the SM with the same mass, the production rate from the top quark contribution is suppressed by at most a few percent due to a slightly smaller top

Yukawa coupling. At next-to-next-to-leading-order in QCD, the SM cross section to produce a 475 GeV Higgs boson at the LHC is about 7 pb [40, 41, 42]. For values of the Higgs mass around 475 GeV, the decay $h \rightarrow ZZ \rightarrow 4\ell$ is the “gold-plated” mode for discovery at the LHC [43].

We also predict a new colored fermion χ that mixes with the top quark and has a mass in the window 1.6 to 2.9 TeV. Since χ is much heavier than the other particles in the SM, the Goldstone boson equivalence theorem implies

$$\Gamma(\chi \rightarrow th) = \Gamma(\chi \rightarrow tZ) = \frac{1}{2} \Gamma(\chi \rightarrow bW) = \frac{\cot^2 \alpha m_t^2}{64 \pi v^2} m_\chi. \quad (64)$$

The total width of χ is approximately 140 GeV for $m_\chi = 2$ TeV. Independently of the mass of the χ field, as long as it is large, it decays to bW with a 50% branching ratio, and to th and tZ with an equal branching ratio of 25%.

The strength of the single χ production rate is governed by $g_{\chi L b_L W}$, which relates to $g_{t_L b_L W}$ by $g_{\chi L b_L W}/g_{t_L b_L W} = \tan \beta_L \approx 0.16$. The single χ production rate is larger than the pair production rate by more than two orders of magnitude when the χ mass is around 2 TeV [44, 45, 46].¹⁶ Therefore, single χ production through the process $qb \rightarrow q'\chi$ provides the best discovery channel at the LHC. Existing studies on new top-like quarks at the LHC show that the χ field can be discovered up to $m_\chi = 2.5$ TeV with 300 fb^{-1} luminosity at a 5σ significance [46] by studying the decay chain $\chi \rightarrow bW \rightarrow \ell\nu b$. This covers a wide range of the expected values of m_χ in this scenario. Specific to our model, the decay chains $\chi \rightarrow ht \rightarrow ZZWb, 3Wb$ and $3W3b$ would provide interesting signal topologies for the presence of the heavy quark and Higgs boson, and deserve more careful studies at the LHC [47].

5 Conclusions

We have considered the intriguing possibility that there may exist a deep connection between two of the known fundamental scales in nature: the Planck and the EW scales. Our framework is based on the observation that the existence of a warped extra-dimension can provide such a deep link through the *dynamical* determination of the ratio between the two scales. As a byproduct, a third scale is *predicted*: the scale of KK resonances.

The scenario we envision is rather economical. No fundamental scalars are introduced, and the 5D version of the SM (without a Higgs) is supplemented by a single $SU(2)_L$ singlet

¹⁶ The coupling among χ , b , and W in our model can be mapped to the $\lambda_1/\lambda_2 = 2$ case in [46].

5D fermion without zero-modes. The EW symmetry is broken as a consequence of top condensation, which results from the strong interactions associated with the lightest KK gluon resonance. In the low-energy theory there appears an effective Higgs degree of freedom with a mass of about 500 GeV and SM-like properties. The fact that the top mass is of order the EW scale is understood as a result of the prominent role the top plays in the breaking of the EW symmetry, as in Topcolor [18] and top seesaw [12] scenarios. Our main observation is that the physics that leads to condensation automatically induces a potential that stabilizes the distance between the UV and IR branes (described by a radion field). Thus, the large hierarchy between the Planck and EW scales is determined dynamically. We showed that this hierarchy is easily obtained without appreciable fine-tuning. More interestingly, when the radion relaxes to the minimum of the potential induced by EW symmetry breaking, the KK scale is determined to be about two orders of magnitude above the EW scale. Although, our analysis was performed in the large N approximation, we believe this is a robust prediction. In particular, the “little hierarchy” between the EW scale (i.e. the top condensation scale) and the KK scale does not correspond to a fine-tuning, but rather to the dynamics of the theory and is related to the fact that $\log M_P/v_{EW} \sim 35$. This latter number results from the fact that the radion relaxation mechanism implies that the coupling of the 4-fermion interaction in the low-energy NJL model is dynamically adjusted to be near the critical value.

The prediction that the KK scale (~ 35 TeV) lies about a factor of 200 above the electroweak scale also allows the scenario to be consistent with EW precision constraints, since corrections due to the KK physics are appropriately suppressed. The negative contribution to the Peskin-Takeuchi T parameter from the 500 GeV Higgs can be compensated by the contribution from a relatively light vector-like quark that mixes with the top quark. In particular, the mass of this new fermion is expected to be between 1.6 and 2.9 TeV, and should be observable at the LHC via single production for most of its expected range. A light radion field with a mass of order a few GeV is also predicted, although its observation is expected to be challenging since it couples weakly to SM matter. Summarizing, the Higgs will be accessible at the LHC with a few fb^{-1} or less, although it will be rather difficult to distinguish it from a SM Higgs. Deviations from the SM in the $ht\bar{t}$ coupling of order 2%, which would induce small variations in the gluon fusion Higgs production and in the Higgs branching fractions, will be most likely beyond the LHC sensitivity given theoretical and experimental uncertainties. This small variation could be probed at a future linear collider. The new light vector-like fermion with mass in the 1.6 – 2.9 TeV range will require LHC integrated luminosities above 100 fb^{-1} , and would be the

first direct new physics signal of this scenario beyond the SM.

It is perhaps somewhat disappointing that the physics ultimately responsible for the radion stabilization mechanism (the KK states) lies beyond the reach of the LHC. On the other hand, the feature that the KK states are rather heavy, might be counted as a success from the point of view of EW precision tests. Notice, however, that the discovery of a vector-like quark with a mass in the TeV range might be taken as indication for the existence of an extra dimension that plays a role in EWSB. A 500 GeV Higgs could suggest the presence of strong dynamics. Our scenario would represent a good example of a natural theory that defies the commonly held expectations that new TeV-scale particles responsible for the cancellation of quadratic divergences in the Higgs boson mass parameter should be present. In the model described in this paper, both the loop contributions to the Higgs mass parameter and the “bare” Higgs mass are of order the KK scale. As emphasized before, the dynamics of our scenario leads to a cancellation between those two contributions, resulting in a Higgs mass of order the electroweak scale.

We also stress that localization of fields in the extra-dimension plays a unifying role in this scenario. The fermions that condense are the two most closely localized near the IR brane. The radion stabilization mechanism drives their 4-fermion interaction strength down, leaving it slightly above criticality and triggering condensation. On the other hand, 4-fermion couplings associated with other fermions not so close to the IR brane are reduced, generically lie below the critical value and do *not* lead to additional bi-fermion condensates. This makes our scenario distinct from previous extra-dimensional realizations of EWSB via fermion-anti fermion condensation [15, 16]. The effective Higgs degree of freedom can be thought as being localized near the IR brane, in the sense that its fermion constituents are. In addition, we showed how all fermion masses other than the top mass can arise from “fundamental” 4-fermion interactions. This results in a scenario where the observed fermion mass hierarchies and flavor structure can be obtained from the localization of the fermions along the extra-dimension, realizing the picture of flavor from anarchy. It is interesting that the same higher-dimensional mechanism of fermion localization can be at the heart of the physics of flavor and EWSB. We find it remarkable that this extremely simple setup can not only explain but also provide rather non-trivial connections between the physics of gravity, EWSB and flavor.

Acknowledgements

We thank Thomas Appelquist, Bogdan Dobrescu, Christopher Hill, Markus Luty and Carlos Wagner for useful comments, and in particular Bill Bardeen for illuminating discussions. E.P. wishes to thank the Fermilab Theory Group for hospitality during various stages of this work. Fermilab is operated by Fermi Research Alliance, LLC under contract no. DE-AC02-07CH11359 with the United States Department of Energy. E.P. was supported by DOE under contract DE-FG02-92ER-40699.

A Validity of the Effective Theory

In the main text we analyzed the low-energy physics associated with the 4-fermion interactions that arise when the KK gluons are integrated out at tree-level. In order for the condensate to form, this coupling needs to be supercritical, hence in the strong-coupling regime. One might then wonder about the reliability of the above results, in particular as regards the radion potential. In this appendix we clarify the precise sense in which the theory is strongly coupled, and argue that in fact the 5D theory provides a calculable UV completion of the above described condensation mechanism. There are two types of effects to consider, associated, respectively, with the KK scale M_{KK} , and with the cutoff of the 5D theory Λ .

We start by discussing the relation between the two scales M_{KK} and $\tilde{\Lambda} = \Lambda e^{-kL}$, and arguing that they are indeed distinct, with $\tilde{\Lambda} \gg M_{\text{KK}}$, in spite of the strong coupling that participates in the condensation mechanism. The important point to realize is that the supercritical coupling, Eq. (10), is obtained by means of localizing the fermion zero-modes very close to the IR brane, not by increasing the 5D gauge coupling g_5 .¹⁷ Furthermore, the localization affects almost exclusively the fermion zero-mode. The fermion KK modes become somewhat heavier when the zero mode is localized closer to the IR brane, while their couplings are rather insensitive to the value of c . For instance, if we concentrate on the physics at the IR brane, where couplings are largest, the KK mode wavefunctions obey $|f_n(L)| \approx \sqrt{2kL}$, essentially independent of c . Recall that, in the KK picture, the large values of these wavefunctions are precisely the reason that the KK modes are more strongly coupled than the zero mode. What is happening as c becomes more negative is that the couplings of the zero mode increase like $f_c(L) \approx \sqrt{(1-2c)kL}$, and

¹⁷In fact, if we identify g_5 with the gauge coupling associated with the SM strong interactions, g_5 is of similar size as in standard RS scenarios with bulk fields (or slightly smaller since one has to match to the 4D gauge coupling at a KK scale of order tens of TeV, as opposed to a few TeV.)

can become as large as those of the KK modes. It follows that only those observables that are IR dominated, hence potentially sensitive to the fermion zero-mode, can be sensitive to the value of c . On the contrary, observables that are UV dominated do not depend on c . This observation will be important when estimating the unknown coefficients of various operators in the underlying 5D theory.

It is instructive to understand the above statements in terms of the fermion propagator in the mixed position/momentum space representation. Considering a fermion with a LH zero-mode, the propagator describing the zero-mode tower takes the form $G_{LL}(y, y') = iP_L \not{p} G_p(y, y')$, where p is the 4-momentum. The exact result for this propagator is given in Eq. (24) of Ref. [30].¹⁸ When considering UV sensitive loops, only the case with $y = y'$ is relevant (non-local effects have an associated Yukawa suppression that ensures they are finite). For illustration purposes we concentrate on the physics near the IR brane, so that $y = y' = L$. In this case, one finds in Euclidean space,

$$G_p(L, L) \approx \frac{e^{4kL}}{p} \left[\frac{1 - c(c+1)\frac{\tilde{k}}{2p}}{1 - c(c-1)\frac{\tilde{k}}{2p}} \right] \rightarrow \frac{e^{4kL}}{p} = \lim_{\Lambda \rightarrow \infty} \int_{-\Lambda}^{\Lambda} \frac{dp_5}{\pi} \frac{e^{4kL}}{p^2 + p_5^2}, \quad (65)$$

where $\tilde{k} = k e^{-kL}$, and the first approximation is excellent for $p \geq \tilde{k}$ and $|c| \leq 1$, which contains the region of interest. We see, as indicated by the arrow, that as soon as p becomes a few times larger than \tilde{k} , the propagator attains its 5D behavior, which is not only independent of c but, as expected, is also identical to the flat space result (the warp factors simply combine to redshift the mass scales appropriately). Thus, UV sensitive loops can be estimated as in *flat* space and are independent of the strong interactions associated with the zero mode when it is localized near the IR brane.

With the above understanding, we proceed to estimate the cutoff of the 5D theory. We define the scale Λ as the lowest scale where an interaction gets strong, understood as the scale where the loop expansion breaks down (adding a loop to a diagram by using the interaction in question does not lead to a suppression). For instance, the fermion one loop contribution to

¹⁸We define the propagators as the inverse of the relevant quadratic operator, \mathcal{O}_2 , including warp factors: $\sqrt{g}\mathcal{O}_2 G = i\delta$. The mixed position/momentum space Feynman rules for the vertices contain also the appropriate warp factors. For instance, for the fermion gauge interactions, one should use $\int dy e^{-3ky} i g_5 \gamma^\mu$, for $\mu = 0, \dots, 3$.

the gluon self-energy is

$$\begin{aligned}
\begin{array}{c} \xrightarrow{q} \\ \text{gluon self-energy diagram} \end{array} &\sim \int dy dy' A_\mu(q, y) P^{\mu\nu} A_\nu(-q, y') N_f g_5^2 \int \frac{d^4 p}{(2\pi)^4} G_p(y, y') G_{|p+q|}(y', y) \\
&\sim \int dy A_\mu(q, y) P^{\mu\nu} A_\nu(-q, y) \left(\frac{N_f g_5^2}{\Lambda} \int \frac{d^4 p}{(2\pi)^4} [G_p(y, y)]^2 \right),
\end{aligned}$$

where N_f is the number of flavors [in the fundamental representation of $SU(N_c)$], and we used that gauge invariance requires the result to be proportional to $P^{\mu\nu} = q^\mu q^\nu - q^2 \eta^{\mu\nu}$. In the second line we used the fact that the propagator $G_p(y, y')$ decays exponentially over distances of order $1/p$, and that the momentum integral is dominated by $p \sim \Lambda$, so that y' is required to be within $1/\Lambda$ of y . Using Eq. (65) for $y = L$, removing the trivial warp factor, and using the indicated cutoff Λ (which corresponds to a truncation of the KK sums), we have $G_p(L, L) = 2 \arctan(\Lambda/p)/(\pi p)$. Using this result, the parenthesis in the above diagram evaluates to $\sim N_f g_5^2 \Lambda / (12\pi^3)$. Notice that the above careful computation using the propagator (65) leads to the same result that one would have obtained in an *uncompactified* 5D theory. The NDA estimate for g_5 then corresponds to

$$g_5^2 \sim \frac{l_5}{N\Lambda}, \quad (66)$$

where $l_5 = 24\pi^3$ is the 5D loop factor,¹⁹ and we replaced $N_f \rightarrow N \equiv |\frac{2}{3}N_f - \frac{5}{3}N_c|$ to take into account the diagrams involving the $SU(N_c)$ self-interactions. Matching to the 4D coupling constant, $g_4^2 = g_5^2/L$, we get

$$\Lambda L \sim \frac{l_5}{N g_4^2}. \quad (67)$$

This result holds both in flat and warped spaces. In warped space, however, we are interested in the relation between Λ and k :

$$\frac{\Lambda}{k} \sim \frac{l_5}{k L N g_4^2}, \quad (68)$$

which for $kL \sim 30$ and $g_4 \sim 0.9$ gives $\Lambda/k \sim 30/N$. If we consider the SM strong interactions with the SM field content then $N_f = 2 \times 6 = 12$, $N_c = 3$ and $N = 3$, so that $\Lambda/k \sim 10$.

¹⁹Although in this one-loop diagram one gets a loop factor suppression of $12\pi^2$, in general the “natural” variable in the momentum integrals is $p^2 + p_5^2$, which leads us to define the generic loop factor with an additional factor of $1/2$ [48]. Of course, NDA should be taken with a grain of salt at this level of precision.

This is large enough for the propagators to attain their asymptotic 5D behavior and validates the previous analysis, in particular that divergent integrals can be estimated as in a flat, uncompactified 5D theory. We stress that this estimate is essentially independent of the strong localization of certain light fields towards the IR brane, and the validity of the 5D theory is as well justified as in other RS scenarios with SM fields in the bulk.

Having established that the cutoff Λ is well above the KK scale, we can estimate the coefficients of various operators in the underlying 5D theory. In the main text, we considered the effects of 4-fermion operators induced at the KK scale. However, one can also write directly 4-fermion operators in the 5D theory:

$$\mathcal{L}_5 \supset \frac{d_{ijkl}}{\Lambda^3} (\bar{\Psi}_i \Gamma \Psi_j) (\bar{\Psi}_k \Gamma \Psi_l) , \quad (69)$$

where the Γ 's are arbitrary matrices and the indices i, j, \dots run over all the fermions. These include the N_f quark flavors as well as any additional $SU(N_c)$ singlets (leptons). Considering the one-loop self-renormalization of the 4-fermion interactions, and assuming that the dimensionless coefficients $d_{ijkl} \sim d$ are all of the same order, we estimate

$$\begin{array}{c} i \quad m \\ \diagdown \quad \diagup \\ \text{---} \text{---} \text{---} \text{---} \\ \diagup \quad \diagdown \\ j \quad n \quad k \quad l \end{array} \sim \sum_{m,n} \frac{1}{l_5} \frac{d_{ijmn}^* d_{klmn}}{\Lambda^3} \sim \left(\frac{n d}{l_5} \right) \frac{d}{\Lambda^3} .$$

Comparing to the tree-level 4-fermion interaction, we see that the NDA estimate for d is l_5/n , where n counts the number of diagrams that can contribute to the loop. The 4-fermion interaction also renormalizes the gluon self-energy considered above, e.g.

$$\begin{array}{c} i \quad j \\ \text{---} \text{---} \text{---} \text{---} \\ \diagdown \quad \diagup \\ \text{---} \text{---} \text{---} \text{---} \\ \diagup \quad \diagdown \\ i \quad j \end{array} \sim \left(\frac{N_f d}{l_5} \right) \left(\frac{N_f g_5^2}{l_5} \Lambda q^2 \right) ,$$

where we indicated schematically the dependence on the external momentum required by gauge invariance. Using the NDA estimate for d , we see that this contribution is suppressed compared to the diagrams that do not involve the 4-fermion interaction by a factor N_f/n , which is typically much smaller than one. We therefore see that the gauge interactions are expected to be stronger than the 4-fermion interactions and should be used to estimate the cutoff Λ , as done above. It is easy to check that this picture holds at higher loop orders.

We can now estimate the size of the above 4-fermion interactions in the low-energy 4D theory:

$$\mathcal{L}_4 \supset \frac{d f_{ijkl}}{(\Lambda L) \tilde{\Lambda}^2} (\bar{\psi}_i \Gamma \psi_j) (\bar{\psi}_k \Gamma \psi_l) , \quad (70)$$

where $\tilde{\Lambda} = \Lambda e^{-kL}$, and $f_{ijkl} = (1/L) \int dy e^{2k(y-L)} f_{c_i} f_{c_j} f_{c_k} f_{c_l}$ contains the dependence on the zero-mode wavefunctions given in Eq. (2). For the fermions that are localized near the IR brane, one has $f_{ijkl} \approx [(\frac{1}{2} - c)^2 / (1 - c)] kL$, where we took, for simplicity, a common localization parameter c . Thus, this 4-fermion operator is suppressed compared to (4) by

$$\frac{d f_{ijkl}}{g_\psi^2} \left(\frac{k}{\Lambda} \right) \left(\frac{M_{\text{KK}}}{\tilde{\Lambda}} \right)^2 \sim g_4^4 (3 - 2c) \left(\frac{N^3}{n} \right) \left(\frac{kL}{l_5} \right)^2 kL, \quad (71)$$

where we used the leading order term for $g_\psi^2 = g_{c_1} g_{c_2}$ from Eq. (10), with $c_1 = c_2 = c$, and the NDA estimates for g_5^2 , d and Λ discussed above. Using $kL \approx 30$, $c \sim -1/2$, $N = 3$, this gives a suppression $\sim 3.5/n$. The number of contributing diagrams, n , depends on the type of operator we are considering. For instance, for the operators considered in Subsection 3.3 that are responsible for giving masses to the fermions other than the top: $(Q_{1L} f_{2R})(Q_{3L} f_{4R})$ where the Q_i 's are $SU(2)_L$ doublets and the f_i 's are $SU(2)_L$ singlets, we typically have $n = 3 \times 4 \times N_c + 3 \times 3 = 45$ [the first term counts quarks, three doublets and four singlets including the additional χ field, the second counts the leptons]. We therefore see that these incalculable effects are expected to be subdominant in regards to the physics that leads to fermion condensation. However, notice that these 4-fermion operators can be included in the analysis of condensation and radion stabilization together with those induced by KK gluon exchange. They simply correspond to adding a new (small) contribution to the c -dependent function of Eq. (7), $f_1(c_1, c_2)$, while leaving $f_2(c_1, c_2)$ in (8) unchanged [see the expression for f_{ijkl} above Eq. (71), or also Eq.(57)]. Thus, the mechanism described in the main text is expected to change only in small details.

B The S and T parameters

In this appendix we collect the formulas for the contributions to the S and T parameters in our model, ΔS and ΔT . These are defined as the deviation from the SM with a fixed reference Higgs mass. There are two main sources for non-zero ΔS and ΔT : one from the vector-like $SU(2)_L$ singlet fermion that mixes with the LH top, and a second one from the fact that the Higgs field in our model is heavier than the reference value. The latter effect gives a contribution [49]

$$\begin{aligned} \Delta S_h &= \frac{1}{12\pi} \log \left(\frac{m_h^2}{m_{h_{\text{ref}}}^2} \right), \\ \Delta T_h &= -\frac{3}{16\pi \cos^2 \theta_W} \log \left(\frac{m_h^2}{m_{h_{\text{ref}}}^2} \right), \end{aligned} \quad (72)$$

where $m_{h_{\text{ref}}} = 117$ GeV is the reference Higgs boson mass, and θ_W is the weak mixing angle. The contribution due to the fermion loop is [50]

$$\begin{aligned}\Delta T_f &= \frac{3 s_{\beta_L}^2}{16\pi \sin^2 \theta_W \cos^2 \theta_W} [W_1(y_\chi, y_b) - W_1(y_t, y_b) - c_L^2 W_1(y_t, y_\chi)] , \\ \Delta S_f &= \frac{3 s_{\beta_L}^2}{2\pi} [W_2(y_\chi, y_b) - W_2(y_t, y_b) - c_L^2 W_3(y_t, y_\chi)] ,\end{aligned}\quad (73)$$

where $y_i \equiv m_i^2/M_Z^2$, and s_{β_L} , c_{β_L} are short notations for $\sin \beta_L$ and $\cos \beta_L$, with β_L the mixing angle of the LH top quarks:

$$\beta_L = \frac{1}{2} \arctan \frac{2 \cos \alpha m_d \bar{g}_{Q_{XR}} \langle H_1 \rangle}{m_d^2 - \bar{g}_{Q_{XR}}^2 \langle H_1 \rangle^2} ,\quad (74)$$

obtained by diagonalization of Eq. (49). Here the functions W_1 , W_2 and W_3 are defined by

$$\begin{aligned}W_1(y_1, y_2) &\equiv y_1 + y_2 - \frac{2 y_1 y_2}{y_1 - y_2} \log \frac{y_1}{y_2} , \\ W_2(y_1, y_2) &\equiv \frac{22 y_1 + 14 y_2}{9} - \frac{1}{9} \log \frac{y_1}{y_2} + \frac{11 y_1 + 1}{18} W_4(y_1, y_1) + \frac{7 y_2 - 1}{18} W_4(y_2, y_2) , \\ W_3(y_1, y_2) &\equiv \frac{y_1 + y_2}{2} - \frac{(y_1 - y_2)^2}{3} + \left(\frac{(y_1 - y_2)^3}{6} - \frac{1 y_1^2 + y_2^2}{2 y_1 - y_2} \right) \log \frac{y_1}{y_2} + \frac{y_1 - 1}{6} W_4(y_1, y_1) \\ &\quad + \frac{y_2 - 1}{6} W_4(y_2, y_2) + \left(\frac{1}{3} - \frac{y_1 + y_2}{6} - \frac{(y_1 - y_2)^2}{6} \right) W_4(y_1, y_2) ,\end{aligned}\quad (75)$$

with

$$W_4(y_1, y_2) \equiv \begin{cases} -2\sqrt{\Delta} (\arctan \frac{y_1 - y_2 + 1}{\sqrt{\Delta}} - \arctan \frac{y_1 - y_2 - 1}{\sqrt{\Delta}}) & \Delta > 0 \\ \sqrt{-\Delta} \log \frac{y_1 + y_2 - 1 + \sqrt{-\Delta}}{y_1 + y_2 - 1 - \sqrt{-\Delta}} & \Delta \leq 0 \end{cases} ,\quad (76)$$

and

$$\Delta = -1 - y_1^2 - y_2^2 + 2 y_1 + 2 y_2 + 2 y_1 y_2 .\quad (77)$$

Other than W_2 , all $W_i(y_1, y_2)$ are symmetric functions under the interchange of the variables y_1 and y_2 .

While both the Higgs and fermion loops give a positive contribution to $\Delta S = \Delta S_h + \Delta S_f$, the contribution to $\Delta T = \Delta T_h + \Delta T_f$ from the Higgs boson is negative and can be compensated by the positive contribution due to the fermions. In our model, since $M_{\text{KK}} \approx 35$ TeV is much larger than the electroweak scale, we neglect the tree-level contributions to the T and S parameters that arise when the KK gauge bosons are integrated out. Other contributions to the T parameter coming from purely LH 4-fermion interactions, as discussed in [51], are negligible.

References

- [1] S. Weinberg, Phys. Rev. D **13**, 974 (1976).
- [2] L. Susskind, Phys. Rev. D **20**, 2619 (1979).
- [3] E. Eichten and K. D. Lane, Phys. Lett. B **90**, 125 (1980).
- [4] S. Dimopoulos and L. Susskind, Nucl. Phys. B **155**, 237 (1979).
- [5] T. Appelquist, M. Piai and R. Shrock, Phys. Rev. D **69**, 015002 (2004) [arXiv:hep-ph/0308061].
- [6] Y. Nambu. Quasisupersymmetry, bootstrap symmetry breaking and fermion masses. Invited talk to appear in Proc. of 1988 Int. Workshop New Trends in Strong Coupling Gauge Theories, Nagoya, Japan, Aug 24-27, 1988.
- [7] V. A. Miransky, M. Tanabashi and K. Yamawaki, Phys. Lett. B **221**, 177 (1989).
- [8] V. A. Miransky, M. Tanabashi and K. Yamawaki, Mod. Phys. Lett. A **4**, 1043 (1989).
- [9] W. J. Marciano, Phys. Rev. D **41**, 219 (1990).
- [10] W. J. Marciano, Phys. Rev. Lett. **62**, 2793 (1989).
- [11] W. A. Bardeen, C. T. Hill and M. Lindner, Phys. Rev. D **41**, 1647 (1990).
- [12] B. A. Dobrescu and C. T. Hill, Phys. Rev. Lett. **81**, 2634 (1998) [arXiv:hep-ph/9712319]; R. S. Chivukula, B. A. Dobrescu, H. Georgi and C. T. Hill, Phys. Rev. D **59**, 075003 (1999) [arXiv:hep-ph/9809470].
- [13] H. J. He, C. T. Hill and T. M. P. Tait, Phys. Rev. D **65**, 055006 (2002) [arXiv:hep-ph/0108041].
- [14] B. A. Dobrescu, Phys. Lett. B **461**, 99 (1999) [arXiv:hep-ph/9812349].
- [15] H. C. Cheng, B. A. Dobrescu and C. T. Hill, Nucl. Phys. B **589**, 249 (2000) [arXiv:hep-ph/9912343].
- [16] N. Rius and V. Sanz, Phys. Rev. D **64**, 075006 (2001) [arXiv:hep-ph/0103086].

- [17] G. Burdman and L. Da Rold, JHEP **0712**, 086 (2007) [arXiv:0710.0623 [hep-ph]].
- [18] C. T. Hill, Phys. Lett. B **266**, 419 (1991).
- [19] C. T. Hill and E. H. Simons, Phys. Rept. **381**, 235 (2003) [Erratum-ibid. **390**, 553 (2004)] [arXiv:hep-ph/0203079].
- [20] T. Gherghetta and A. Pomarol, Nucl. Phys. B **586**, 141 (2000) [arXiv:hep-ph/0003129].
Y. Grossman and M. Neubert, Phys. Lett. B **474**, 361 (2000) [arXiv:hep-ph/9912408].
- [21] L. Randall and R. Sundrum, Phys. Rev. Lett. **83**, 3370 (1999) [arXiv:hep-ph/9905221].
- [22] W. D. Goldberger and M. B. Wise, Phys. Rev. Lett. **83**, 4922 (1999) [arXiv:hep-ph/9907447].
- [23] E. Pontón and E. Poppitz, JHEP **0106**, 019 (2001) [arXiv:hep-ph/0105021].
- [24] Y. Nambu and G. Jona-Lasinio, Phys. Rev. **122**, 345 (1961); Phys. Rev. **124**, 246 (1961).
- [25] A. Jenkins, Phys. Rev. D **69**, 105007 (2004) [arXiv:hep-th/0311127].
- [26] M. S. Carena, E. Pontón, T. M. P. Tait and C. E. M. Wagner, Phys. Rev. D **67**, 096006 (2003) [arXiv:hep-ph/0212307].
- [27] R. Barbieri and G. F. Giudice, Nucl. Phys. B **306**, 63 (1988).
- [28] G. W. Anderson and D. J. Castaño, Phys. Lett. B **347**, 300 (1995) [arXiv:hep-ph/9409419].
- [29] C. Amsler et al., Phys. Lett. B **667**, 1 (2008)
- [30] M. S. Carena, A. Delgado, E. Pontón, T. M. P. Tait and C. E. M. Wagner, Phys. Rev. D **71**, 015010 (2005) [arXiv:hep-ph/0410344].
- [31] E. W. Varnes, Plenary talk, 34th International Conference on High-Energy Physics (ICHEP), 2008.
- [32] W. D. Goldberger and M. B. Wise, Phys. Lett. B **475**, 275 (2000) [arXiv:hep-ph/9911457].
- [33] G. F. Giudice, R. Rattazzi and J. D. Wells, Nucl. Phys. B **595**, 250 (2001) [arXiv:hep-ph/0002178].

- [34] C. Csaki, J. Hubisz and S. J. Lee, Phys. Rev. D **76**, 125015 (2007) [arXiv:0705.3844 [hep-ph]].
- [35] P. D. Acton *et al.* [OPAL Collaboration], Phys. Lett. B **268**, 122 (1991).
- [36] Z. Han, Phys. Rev. D **73**, 015005 (2006) [arXiv:hep-ph/0510125].
- [37] M. S. Carena, E. Pontón, J. Santiago and C. E. M. Wagner, Phys. Rev. D **76**, 035006 (2007) [arXiv:hep-ph/0701055].
- [38] A. Djouadi, M. Spira and P. M. Zerwas, Z. Phys. C **70**, 427 (1996) [arXiv:hep-ph/9511344].
- [39] A. Djouadi, J. Kalinowski and M. Spira, Comput. Phys. Commun. **108**, 56 (1998) [arXiv:hep-ph/9704448].
- [40] S. Catani, D. de Florian, M. Grazzini and P. Nason, JHEP **0307**, 028 (2003) [arXiv:hep-ph/0306211].
- [41] M. S. Carena and H. E. Haber, Prog. Part. Nucl. Phys. **50**, 63 (2003) [arXiv:hep-ph/0208209].
- [42] A. Djouadi, Phys. Rept. **457**, 1 (2008) [arXiv:hep-ph/0503172].
- [43] CMS Technical Design Report, <http://cmsdoc.cern.ch/cms/cpt/tdr/>
- [44] T. Han, H. E. Logan, B. McElrath and L. T. Wang, Phys. Rev. D **67**, 095004 (2003) [arXiv:hep-ph/0301040].
- [45] M. Perelstein, M. E. Peskin and A. Pierce, Phys. Rev. D **69**, 075002 (2004) [arXiv:hep-ph/0310039].
- [46] G. Azuelos *et al.*, Eur. Phys. J. C **39S2**, 13 (2005) [arXiv:hep-ph/0402037].
- [47] Y. Bai, M. Carena, B. Panes and E. Pontón, in preparation.
- [48] Z. Chacko, M. A. Luty and E. Pontón, JHEP **0007**, 036 (2000) [arXiv:hep-ph/9909248].
- [49] M. E. Peskin and T. Takeuchi, Phys. Rev. D **46**, 381 (1992).
- [50] L. Lavoura and J. P. Silva, Phys. Rev. D **47**, 1117 (1993).
- [51] R. S. Chivukula and H. Georgi, Phys. Rev. D **58**, 075004 (1998) [arXiv:hep-ph/9805478].